



KAUNAS UNIVERSITY OF TECHNOLOGY
FACULTY OF ELECTRICAL AND ELECTRONICS ENGINEERING

Damira Smagulova

**ULTRASONIC NON-DESTRUCTIVE EVALUATION OF
DISSIMILAR MATERIAL JOINTS**

Final project for Master degree

Supervisor

Assoc. Prof. Dr. Elena Jasiuniene

KAUNAS, 2015

KAUNAS UNIVERSITY OF TECHNOLOGY
FACULTY OF ELECTRICAL AND ELECTRONICS ENGINEERING

**ULTRASONIC NON-DESTRUCTIVE EVALUATION OF
DISSIMILAR MATERIAL JOINTS**

Final project for Master degree
Measurement Engineering (code 621H14001)

Supervisor

(signature) Assoc. Prof. Dr. Elena Jasiuniene
(date)

Reviewer

(signature)
(date)

Project made by

(signature) Damira Smagulova
(date)

KAUNAS, 2015



KAUNAS UNIVERSITY OF TECHNOLOGY

Faculty of Electrical and Electronics Engineering

(Faculty)

Damira Smagulova

(Student's name, surname)

Measurement Engineering (621H14001)

(Title and code of study programme)

"Ultrasonic non-destructive evaluation of dissimilar material joints"

DECLARATION OF ACADEMIC HONESTY

_____ 20
_____ Kaunas

I confirm that a final project by me, **Damira Smagulova**, on the subject "Ultrasonic non-destructive evaluation of dissimilar material joints." is written completely by myself; all provided data and research results are correct and obtained honestly. None of the parts of this thesis have been plagiarized from any printed or Internet sources, all direct and indirect quotations from other resources are indicated in literature references. No monetary amounts not provided for by law have been paid to anyone for this thesis.

I understand that in case of a resurfaced fact of dishonesty penalties will be applied to me according to the procedure effective at Kaunas University of Technology.

(name and surname filled in by hand)

(signature)

Smagulova, D. Ultrasonic non-destructive evaluation of dissimilar material joints. Final project for *master degree* / supervisor Assoc. Prof. Dr. Elena Jasiuniene; Kaunas University of Technology, Faculty of Electrical and Electronics engineering, department of electric and electronics.

Kaunas, 2015. 79 p.

SUMMARY

On the present work the quality of joint of dissimilar materials was inspected using ultrasonic waves. Various ultrasonic techniques and sample characteristics were analyzed to develop suitable configuration for the inspection of joint of dissimilar materials. Using CIVA software the sample was designed and virtual ultrasonic inspections performed using conventional, focused and phased array transducers with a frequency range from 3,5 MHz to 10 MHz. Suitable type and frequencies of ultrasonic transducer as well as the side of the sample from which the inspection has to be performed are selected according to results of CIVA modelling. Using Omniscan measurement system and phased array transducers of 3,5 MHz and 5 MHz the delaminations between dissimilar joints were found experimentally. The lengths of delaminations and their depths were measured and compared to theoretically calculated values. Using Tecscan measurement system and immersion transducers the location of defects was determined. The uncertainties of results of ultrasonic testing were estimated.

CONTENTS

INTRODUCTION.....	6
1 ANALYSIS OF ULTRASONIC METHODS SUITABLE FOR THE INSPECTION OF JOINTS OF DISSIMILAR MATERIALS.....	7
1.1 Pulse Echo method.....	7
1.2 Trough–Transmission Technique.....	8
1.4 Lamb wave testing.....	9
1.5 Resonance Technique.....	10
1.6 Acousto-Ultrasonic Technique.....	11
1.7 Selection of the most suitable ultrasonic method for the inspection of joints of dissimilar materials.....	12
2 DESCRIPTION AND CHARACTERISTICS OF THE OBJECT AND ULTRASONIC TRANSDUCERS.....	14
2.1 Specimen parameters and its defects.....	14
2.2 Characteristics of conventional and phased array transducers.....	15
3 CIVA COMPUTER MODELING OF JOINT OF DISSIMILAR MATERIALS.....	17
3.1 Water path calculation of the transducers.....	18
3.2 Investigation of ultrasonic field of different transducers in CIVA software.....	20
3.2.1 Sample inspection from composite side.....	21
3.2.2 Sample inspection from metal side.....	22
3.3 Estimation of the reflection coefficients.....	24
3.4 Investigation of sample with defects in CIVA software.....	24
3.4.1 Sample inspection from composite side.....	26
3.4.2 Sample inspection from metal side.....	30
3.5 CIVA investigation of the attenuation influence.....	35
3.6 Conclusions.....	36
4 EXPERIMENTAL EVALUATIONS.....	37
4.1 Ultrasonic velocity measurement.....	37
4.2 Parameters and characteristics of the inspection of defects with phased array transducers.....	40
4.3 Defect inspection of the joint of steel and GFRP with 5 MHz phased array transducer.....	42
4.4 Defect inspection of the joint of steel and GFRP with 3,5 MHz phased array transducer.....	45
4.5 Sample inspection using trough-transmission method.....	48
4.6 Conclusions.....	51
5 EVALUATION OF THE UNCERTAINTY OF THE MEASUREMENT RESULTS.....	52
5.1 Probability of detection curves computation in CIVA software.....	52
5.2 Uncertainty evaluation of experimental ultrasonic testing.....	54
CONCLUSIONS.....	70
APPENDIX.....	74
Appendix 1. Scientific article of 12th student’s conference E2TA on the topic of “Ultrasonic non-destructive evaluation of dissimilar material joints”.....	74

INTRODUCTION

Ultrasonic non-destructive testing (NDT) is widely used for the inspection of different types of materials. Ultrasonic instruments and software allows quickly detect flaws; determine their types, geometry, dimensions and the danger which defects bring to the object [1].

Adhesively bonded dissimilar materials have a great interest in various fields of industry as aerospace, shipbuilding, energetic, construction and other areas of manufacturing. Variety of adhesively bonded metal and composite materials is employed in aerospace for commercial and military aircrafts. In particular, bonded joints of metal and aramid, carbon and glass fibre reinforced plastics are used for aircraft wings, tail and other parts. The use of this kind of structures leads to a reduction of aircraft weight as well as to strength and rigidity increase [2], [3].

In adhesively bonded materials different types of defects as large bubbles, voids and porosity can occur by a lack of adhesive or by the presence of foreign objects. The major problem is delaminations which are caused by poor joining.

All new joints of dissimilar materials require suitable ultrasonic technique of the inspection which has to be developed. Different parameters and characteristics as object geometry, structure, dimension, thickness, material properties as well as possible types of defects affect on the choice of ultrasonic technique [4], [5]. Therefore, to select suitable ultrasonic technique all these characteristics and parameters have to be studied.

The aim of this thesis is to evaluate the joint of dissimilar materials between steel and glass fibre reinforced plastic (GFRP) using ultrasonic non-destructive method.

The subject of this study is investigation of quality of bonding layer of joints of dissimilar materials using ultrasound waves. The object of the study is the presence of delaminations in the sample.

To achieve the objective of this investigation project the following tasks are going to be studied:

- analysis of ultrasonic methods which are suitable for the examination of joints of dissimilar materials, as well as the choice of the appropriate method for a given sample;
- computer modelling using CIVIA software in order to investigate influence of various factors for non-destructive evaluation of dissimilar joints;
- ultrasonic investigation of dissimilar material joints experimentally.

For the validity of research done the calculations of uncertainty of the results will be performed.

1 ANALYSIS OF ULTRASONIC METHODS SUITABLE FOR THE INSPECTION OF JOINTS OF DISSIMILAR MATERIALS

There are several main ultrasonic techniques of the object inspection in ultrasonic NDT. The choice of the method depends on geometry and dimension of the object under inspection, its structure, properties and surface condition as well as on the inspection conditions [5].

Suitable ultrasonic technique has to be developed for the inspection of joint of steel and GFRP. So to achieve this goal main methods of ultrasonic inspection are analyzed in this part of thesis.

1.1 Pulse Echo method

Ultrasonic Pulse Echo method is a well-established technique which is widely used in non-destructive testing. Ultrasonic transducer transmits repetitive acoustic pulses to the adhesively bonded joints of dissimilar materials. The acoustic pulses reflect from the bonding or various defects and the same transducer receives these signals (echoes). The propagation of acoustic waves in joint of steel and GFRP is shown in **Fig.1.1**.

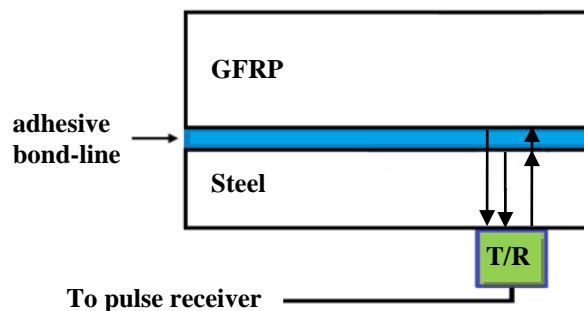


Fig.1.1. Pulse echo inspection of adhesive bonds of dissimilar materials [8]

The direction of the reflected ultrasound signal depends on incidence angle of transducer as well as on the orientation of the reflecting defect or surfaces of the sample. Received ultrasound signals are monitored on display of measurement instrument. The amplitude of signal and time delay between initial pulse and received pulse are measured [1], [7].

Amplitude scans (A-scans) of the inspection of quality of adhesively bonded materials are shown in **Fig.1.2**. As a result a portion of energy will be reflected back to transducer and other portion will be transmitted in to the bonded layer and absorbed each time when ultrasound signal reaches the interface of the object. In the case of void presence all the energy of ultrasound will be reflected back to transducer. The attenuation of ultrasound signals reflected from the interface

of good bond will be higher than attenuation of signals reflected from the unbonded area. In addition to that for an unbonded layer the amplitude of each ultrasound reflection will be slightly bigger because there is no interface loss of energy [6].

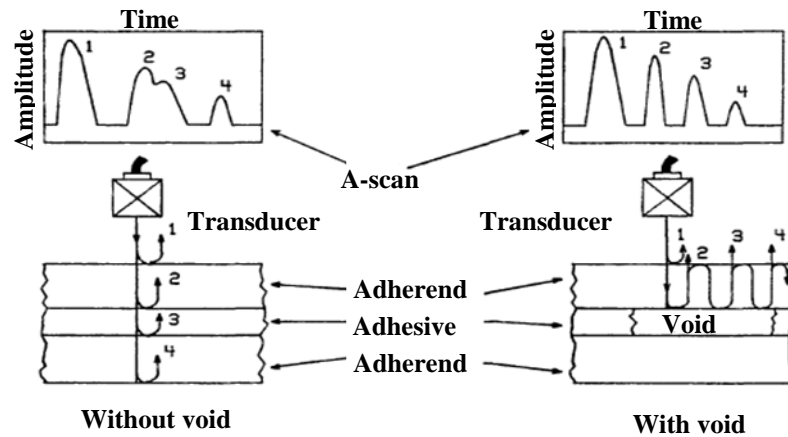


Fig.1.2. A-scans of the inspection of quality of adhesively bonded materials [6]

Advantages: pulse echo inspection can be performed with longitudinal, shear, surface or Lamb waves; straight beam or angle beam techniques can be used to detect defects of different orientation; type, location, size and orientation of defects can be determined from the data; separate transmitting and receiving transducers can be used. Disadvantages: defects can't be detected in the region where time period equals to the wavelength of ultrasound (dead zone) [4], [7]-[9].

1.2 Through-Transmission Technique

The through-transmission technique is performed using separate transmitting and receiving probes on either side of the joint of dissimilar materials as it shown in **Fig.1.3**. The position of two transducers has to be exactly one in front another. Water or special gels can be used as a coupling media between transducers and the joint of dissimilar materials in ultrasonic non-destructive techniques. The contact through-transmission technique is used in practice very rare because of the complexity to align probes one in front another and the requirement of access to the both sides of the object and good contact. Immersion through-transmission method has more popularity, transmitting and receiving probes are fixed and scanning the sample along a predetermined axis. For the defect detection the magnitude of transmitted signal is monitored on C-scan which produces two-dimensional image of defects in the sample. In the case of defect presence the amplitude of the received signal is lower than the amplitude of the signal received from the area without defect.

Through-transmission technique is widely used for the detection of discontinuities. The presence of defects can be determined by amplitude analysis of the received signals [4], [6].

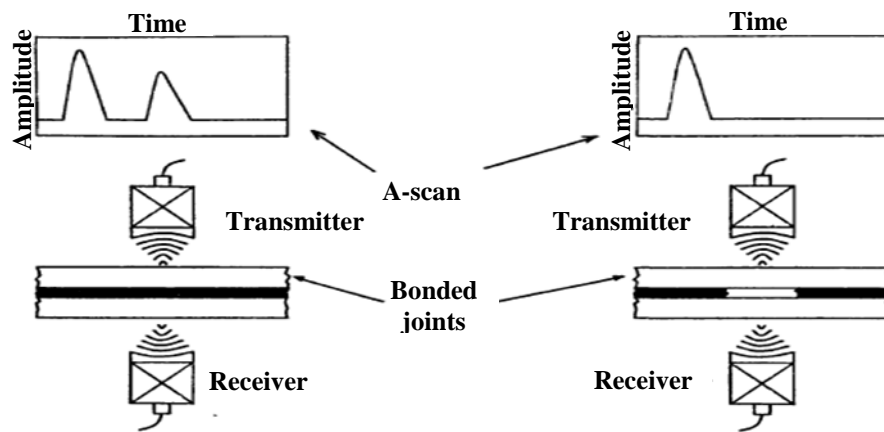


Fig.1.3. Ultrasonic through-transmission technique [6]

Advantages: detection of most common defects; there is no dead zone. Disadvantages: impossibility of defect depth detection; not suitable for specimens that can be investigated only from one side; difficult to position transducers exactly one in front another [4], [6], [10].

1.4 Lamb wave testing

Lamb waves are used for the high speed testing of a plate, wire, strip and other thin materials. Lamb waves propagate only in the plates with a thickness comparable to the wavelength. In this case the complex resonance phenomena occur in plate and leads to the formation of standing waves. Lamb waves or (plate waves) are complex elastic waves which are propagating in an elastic medium formed by the combination of standing and guided waves. Lamb waves consist of different modes moving at different speeds [11], [12]. Most common propagation modes are symmetrical and asymmetrical modes which are shown in **Fig.1.4**.

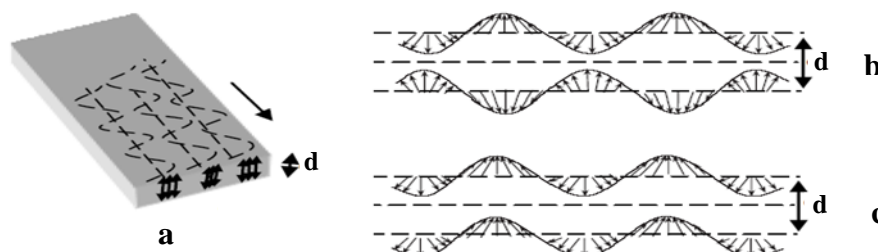


Fig.1.5. Propagation modes of Lamb waves: a-propagation of Lamb waves in a plate of thickness d , b-symmetric mode, c-asymmetric mode [11]

In the case of propagation of symmetric mode the plate surface moves in opposite side, in the case of propagation of asymmetric mode the plate surface moves in one direction. The speed of Lamb wave propagation depends on the modes and the thickness of the plate [11].

The experimental set-up of Lamb wave testing of adhesively bonded joint is shown in **Fig.1.5**.



Fig.1.5. Experimental set-up of Lamb wave testing of adhesively bonded joints [11]

Two immersion transducers with 500 kHz central frequency one as transmitter and another as receiver in a pitch and catch configuration were used. Each transducer is connected to a rotation stage to control the inclination. For excitation of desirable mode the particular angle of transducer inclination was selected and fixed. Immersion method was performed to guarantee the same coupling between the transducers and the plate. The ultrasonic signal was transmitted to the plate and after propagation the ultrasound collected by the receiver. In the next steps the signal was amplified and filtered. In order to increase signal to noise ratio the signal was averaged by oscilloscope and transferred to a computer for processing and analyzing [11].

Advantages: high-speed testing of thin materials, whose thickness is equal to a few wavelengths; can test material at various angles of incidence in the frequency range of 0,1 to 15,0 MHz; propagation at long distances. Disadvantages: active driving mechanism requirement for wave propagation; complexity to interpret the resulting data [11], [12], [13].

1.5 Resonance Technique

Resonance technique is based on the changing of frequency of acoustic wave until the resonance condition is occurred. Resonance technique of the inspection of adhesively bonded materials is shown in **Fig.1.6**. As a result during the resonance standing waves were generated in the case of good bond and void between materials. The length of standing wave at resonance frequency is calculated according to the equation:

$$\lambda_D = 2D = \frac{c}{f_D}, \quad (1.1)$$

Where λ_D is the length of the standing wave in the joint area, D is the thickness of the joint, c is the velocity of sound waves in the adherends (the thin adhesive layer is neglected) and f_D is the resonant frequency.

In the case of presence of void the resonant frequency will change sharply comparing to resonant frequency of good bond due to change of thickness value [6], [14].

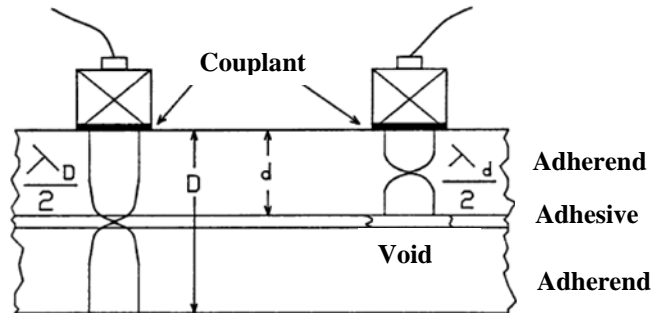


Fig.1.6. Resonance Technique [6]

Advantages: thickness measurements; defect detection in adhesive areas of the joints; low cost. Disadvantages: low frequency range of 20 Hz; difficult to detect small defects and geometric deviations because of little influence on resonant frequency; depends on object geometry and structure [6], [14].

1.6 Acousto-Ultrasonic Technique

The acousto-ultrasonic technique of non-destructive testing can be used to provide information about the presence of various defects in specimens and quality of adhesively bonded dissimilar materials by correlating characteristics of propagation of stress waves with the the strength of the joint [1].

In this technique a broadband transducer is used as a transmitter of repetitive ultrasonic pulses into the sample. Another transducer is used as a receiver of stress waves occurred from the injected ultrasonic pulses. The receiver is placed on the same side of sample as a transmitter at a specific distance. The longitudinal waves are excited and transmitted perpendicular to the sample surface. The ultrasound waves will produce oblique reflections and shear waves in the material. The resulting stress waves get multiple reflections from the surfaces and interfaces of the sample and interact with different discontinuities. As a result structural performance and presence of various defects can be determined due analysis of stress waves which are affected by

properties of sample microstructure and morphology. In many cases the information of mechanical behaviour is possible to obtain from analysis of data of stress wave propagation [1], [7].

The experimental set-up of acousto-ultrasonic technique is shown in **Fig.1.7**.

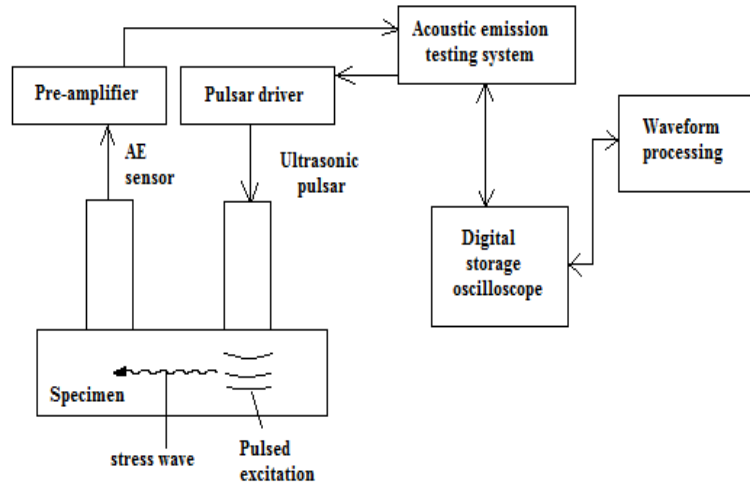


Fig.1.7. Experimental set-up of acousto-ultrasonic technique [1]

Advantages: detection of large flaws, delaminations and material properties; one-side accessibility. Disadvantages: can't be used to detect small, single flaws because of the lack of influence on mechanical properties; the wavelength is much longer than in other ultrasonic methods [1], [6], [15].

1.7 Selection of the most suitable ultrasonic method for the inspection of joints of dissimilar materials

In the case of ultrasonic inspection of the joint of dissimilar materials, the choice of the method and suitable transducer depends on the:

- properties of materials which have to be measured;
- different materials thicknesses;
- object geometry;
- object sizes;
- object structure;
- temperature, accuracy requirements and other inspection conditions [5].

The object to be inspected has a simple planar geometry with a length and width of 300 mm, the thickness of the object is 10,42 mm. One layer is a stainless steel with a thickness of 6,3 mm, other layer is a GFRP with a thickness of 4,12 mm. In **Table 1.1** the wavelengths of ultrasound

in metal and composite using frequency of 3,5 MHz, 5 MHz and 10 MHz are presented and calculated according to equation:

$$\lambda = \frac{c}{f}, \quad (1.2)$$

where λ -wavelength, c -ultrasound velocity in dissimilar materials, f -frequency.

Table 1.1. Parameters of wavelength in different materials

Sample	Frequency f, MHz	Theoretical velocity c, m/s	Wavelength, λ , mm
Steel	3,5	5 940	1,750
GFRP		3 150	0,832
Steel	5	5 940	1,225
GFRP		3 150	0,583
Steel	10	5 940	0,613
GFRP		3 150	0,291

Based on it the thickness of the object is enough large, what prevents the use of Lamb wave testing. The type of the material is very important factor because of different properties; in the case of composite material it absorbs ultrasound waves more quickly comparing to steel, that is why when performing investigation of defects between dissimilar materials from composite side it is better to use not very high frequencies of transducers to avoid the increase of attenuation. Composite has several sublayers arranged at different angles. Due to it waves scattering increases what leads to increased attenuation [5], [16], [17].

Adhesively bonded joints are widely used in different industries and can have several types of defects. The most common defects in such type of joints are delaminations. The types of possible defects and their orientation and sizes which have to be inspected have to be taken into account. Ultrasonic inspection of delaminations of joint of steel and GFRP has to be performed.

The construction and geometry of the object makes possible to inspect it from both sides as well as apply through transmission method. The disadvantage of this method is that it requires transmitting and receiving probes to be positioned on both sides of the joint and to be exactly aligned [4].

Based on the characteristics and conditions described, the pulse-echo method is more simple and effective in implementation using one transducer which is emitter and receiver. The frequency to be used for transducers is chosen according to the type of materials, their thickness; produced wavelength in materials which depends on ultrasonic velocity and frequency; as well as attenuation which leads to amplitude reducing of sound pressure due to friction losses in transmission materials. As a result ultrasonic transducers of 3,5-10 MHz are most suitable for the task.

2 DESCRIPTION AND CHARACTERISTICS OF THE OBJECT AND ULTRASONIC TRANSDUCERS

The object under inspection is a joint of dissimilar materials which has delaminations between composite and metal layer. This kind of structure of the object is widely used in various industries. Therefore, the study of this topic is relevant. In this part of work the parameters and structure of the object is described as well as characteristics of transducers.

2.1 Specimen parameters and its defects

The specimen, that has to be investigated, is a joint between steel and GFRP. There are 3 artificial delaminations in the joint of dissimilar materials. Geometry characteristics of the sample are shown in **Table 2.1**.

Table 2.1. Geometry data of specimen

Shape	Content	Length (a), mm	Width (b), mm	Thickness (c), mm	
				Steel	GFRP
planar	1st layer – glass fiber reinforced plastic, GFRP	300	300	6,30	4,12
	2nd layer - steel			Total: 10,42	

It should be noticed that the thickness of the composite is 4,12 mm (d) and it consists of 4 sub-layers of glass fibre/epoxy resin. The thickness of each composite sub-layer is 1,03 mm. Hence the thickness of steel is 6,30 mm. The geometry parameters of the specimen are illustrated in **Fig. 2.1**.

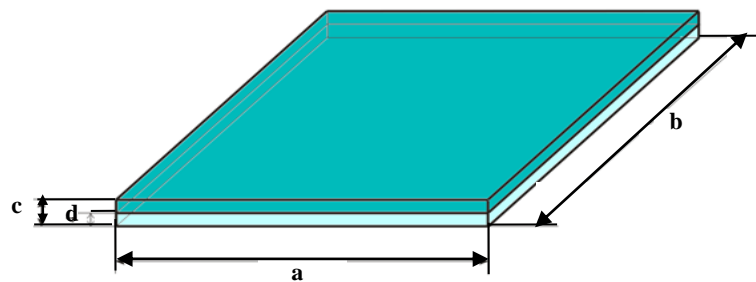


Fig.2.1. Geometry characteristics of the sample

Acoustic properties of steel and GFRP are presented in **Table 2.2**.

Table 2.2. Theoretical properties of dissimilar materials

Material	Theoretical velocity of longitudinal waves c , m/s	Theoretical velocity of transverse waves c , m/s	Acoustic impedance Z , MRayl
Steel	5 940	3 251	45,4
GFRP	3 150	1 727	6,04

Acoustic impedances z of steel and GFRP are defined as a product of their densities ρ and acoustic velocity c . Acoustic impedance plays a significant role in determining the acoustic transmission and reflection at the boundary of two dissimilar materials having different acoustic impedances [18], [19].

2.2 Characteristics of conventional and phased array transducers

The characteristics of conventional and linear phased array transducers which could be used for ultrasonic testing are shown in **Table 2.3** and **Table 2.4** respectively.

Table 2.3. Characteristics of conventional transducers

№	Transducer	Type	Pattern	Shape	Diameter, mm	Focusing	Radius, mm
1	5 MHz transducer	Immersion	Single element	Circular	10	Flat	-
2	10 MHz transducer	Immersion	Single element	Circular	10	Flat	-
3	10 MHz transducer	Immersion	Single element	Circular	10	Spherical	24,5

Table 2.4. Characteristics of phased array transducers

Transducer	3,5MHz transducer (3.5L64-64x7-NW1-P-2.5-OM)	5 MHz transducer (5L128-128x7-NW3-P-2.5-OM)	10 MHz transducer (10L128-64x7-I2-P-2.5-HY)
Pattern	Linear phased array	Linear phased array	Linear phased array
Incident dimension (Virtual aperture A_v), elements	64	128	64
Orthogonal dimension (Passive aperture, W), mm	7	7	7
Number of elements (active aperture A)	64	128	128
Gap between elements (g), mm	0,1	0,1	0,1
Element width (e), mm	0,9	0,9	0,4

Phased array transducers can be employed in almost any cases where conventional transducers are used. The main benefits of phased arrays is steering of multiple elements, focusing, covering and electronically scanning large area of the sample what avoids mechanical scanning using conventional transducers [20]. Parameters of linear phased array transducer are shown in **Fig.2.2**.

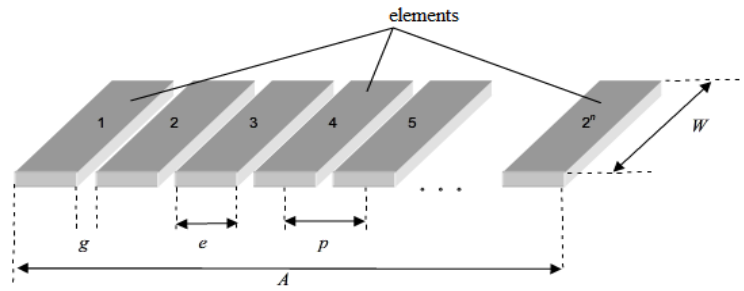


Fig.2.2. Parameters of phased array transducer: A -active aperture; W -passive aperture; e -element width; g -space between elements; p -distance between centres of 2 elements [16]

Characteristics of the Olympus wedges for 3,5 MHz and 5 MHz phased array transducers are given in **Table 2.5**.

Table 2.5. Characteristics of the wedges

Wedge	Nominal Refracted Beam Angle (in Steel)	Probe Orientation	Wedge Dimensions, mm		
			L	W	H
SNW3-0L-IHC-C	0°LW	Normal	130	32	20
SNW1-0L-WP5	0°LW	Normal	66	32	20

3 CIVA COMPUTER MODELING OF JOINT OF DISSIMILAR MATERIALS

In order to find suitable configuration for the inspection of joint of dissimilar materials CIVA software was used. In this program ultrasonic field's radiated by transducers can be visualized and investigated. The object which is under inspection and optimal transducers are designed. In addition CIVA can be used for optimizing strategies of the inspection, verifying its parameters, as well as helping in results analysis [21]. The joint of dissimilar materials was inspected from composite and metal side in order to define better side of the object for ultrasonic inspection of delaminations. Using the toolbox of the program, expected interaction of ultrasonic waves with delaminations in the sample was evaluated.

In this thesis part ultrasonic fields of conventional transducers, focused and phased array transducers are studied.

Properties of steel and GFRP are given in **Table 3.1**.

Table 3.1. Material properties

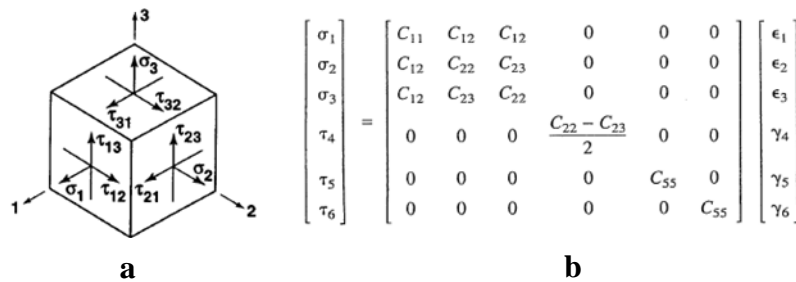
Material	Density ρ , $g.cm^{-3}$	Velocity of longitudinal waves c , m/s	Velocity of transverse waves c , m/s
Steel	7,8	5 900	3 230
Glass fiber	1,67	3 150	1 727
Epoxy	1,23	2 488	1 134

The generalized Hooke's law which is relating stresses to strain:

$$\sigma_i = C_{ij}\varepsilon_j, \quad i, j = 1, \dots, 6 \quad (3.1)$$

Where σ_i are the stress components shown on a three-dimensional cube in x, y, and z coordinates in **Fig.3.1 (a)**, C_{ij} is the stiffness matrix, and ε_j are the strain components.

GFRP is a unidirectional transversely isotropic material or orthotropic material with one of its planes which is a plane of isotropy. At every point of this plane the mechanical properties are the same in all directions [22]. The 1-2 plane is the plane of isotropy, then 1 and 2 subscripts on the stiffness are interchangeable. The stress-strain relations have only five independent elasticity constants and illustrated in **Fig.3.1 (b)**.



a

b

$$\begin{bmatrix} \sigma_1 \\ \sigma_2 \\ \sigma_3 \\ \tau_4 \\ \tau_5 \\ \tau_6 \end{bmatrix} = \begin{bmatrix} C_{11} & C_{12} & C_{12} & 0 & 0 & 0 \\ C_{12} & C_{22} & C_{23} & 0 & 0 & 0 \\ C_{12} & C_{23} & C_{22} & 0 & 0 & 0 \\ 0 & 0 & 0 & \frac{C_{22} - C_{23}}{2} & 0 & 0 \\ 0 & 0 & 0 & 0 & C_{55} & 0 \\ 0 & 0 & 0 & 0 & 0 & C_{55} \end{bmatrix} \begin{bmatrix} \varepsilon_1 \\ \varepsilon_2 \\ \varepsilon_3 \\ \gamma_4 \\ \gamma_5 \\ \gamma_6 \end{bmatrix}$$

Fig.3.1. Stress components (a) and stress-strain relations (b): γ_i -shear strains, τ_i -shear stresses

The matrix of composite material is illustrated in **Fig.3.2 (a)** and positioning of sub-layers of composite material is shown in **Fig.3.2 (b)**.

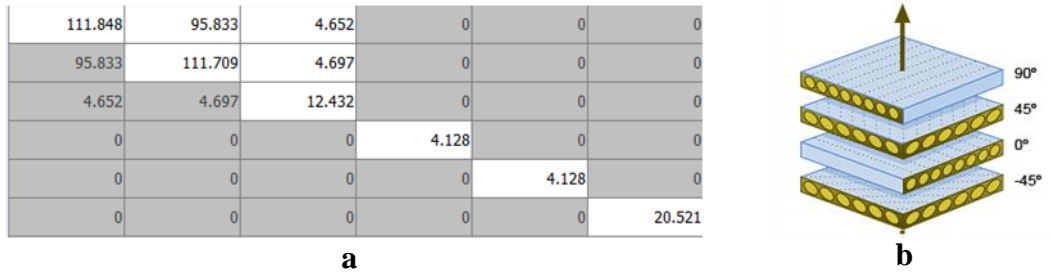


Fig.3.2. Anisotropic matrix of stiffness (a) and composite sub-layer's algorithm (b)

As it shown in Fig.3.2 (b) there are 4 sub-layers of composite material arranged at different angles. Flexural and torsional stiffness depends on order of placing sub-layers. The matrix properties determine the strength of the composition in shear, compression and resistance to fatigue failure [22], [23].

3.1 Water path calculation of the transducers

There are two zones in the field of ultrasonic transducer:

- near field;
- far field.

Big fluctuations of sound pressure occur in near field, which limits the possibility of defect inspection and evaluation of their values. Therefore, defects must be located in far field. The length of the near field is calculated according to the equation:

$$N = \frac{D^2}{4\lambda} = \frac{D^2 f}{4c}, \quad (3.2)$$

where D is a diameter of transducer, f is a frequency of transducer and c is a velocity of ultrasound in the water [16].

Assuming that the speed of sound in water is 1 500 m/s, the diameter of the transducer is 10mm and the frequency 5 MHz, the length of the near field is 84 mm. In the case of 10 MHz transducer, the near field length is 167 mm. Transducers were modelled using CIVA software and the distributions of the amplitude along the transducer's axis of 5 and 10 MHz are shown in **Fig.3.4** and in **Fig.3.5** respectively.

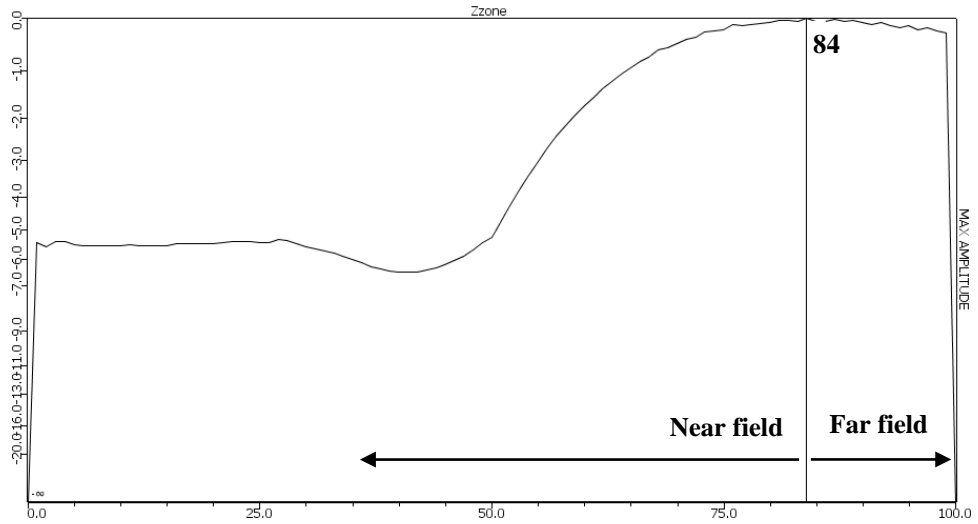


Fig.3.4. The distribution of the amplitude along 5 MHz transducer's axis

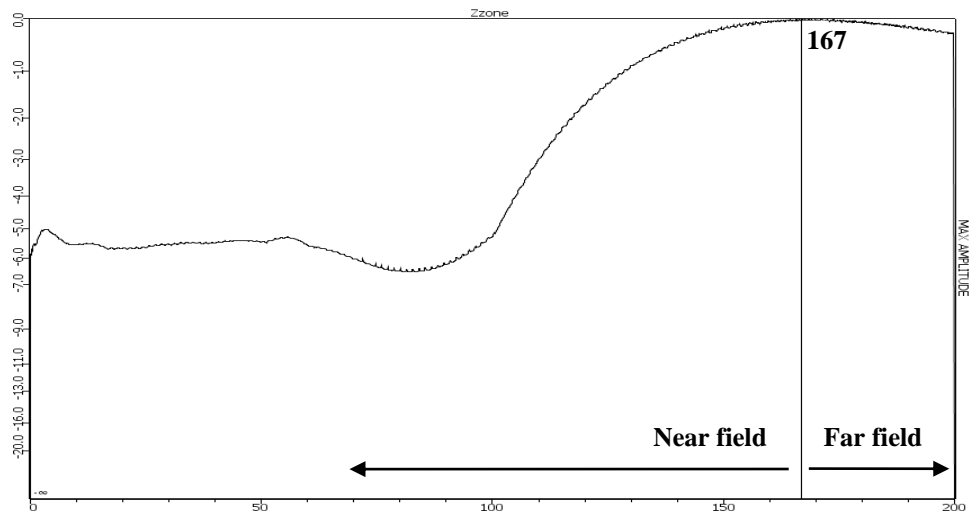


Fig.3.5. The distribution of the amplitude along 10 MHz transducer's axis

Focused transducer concentrates energy of field in a narrow zone. The value of focused zone depends on the frequency of transducer. The maximum amplitude is in the focused zone [16]. The distribution of the amplitude along 10 MHz focused transducer and ultrasonic field in water is shown in **Fig.3.6**. The depth of focus is 49 mm.

For better resolution zone of focus should be in a required area of the sample. Therefore the distance of location of focused transducer is calculated according to the equation:

$$WP = F - MP(c_{mat} / c_{wat}), \quad (3.3)$$

where WP is a water path needed for the inspection of the sample, F is a focal point, MP is material path, c_{mat} is a velocity in material and c_{wat} is a velocity in water [16]. As a result of calculation for sample inspection from composite side the distance between transducer and sample has to be 40,27 mm; in the case of inspection from metal side the distance equals to 23,93 mm.

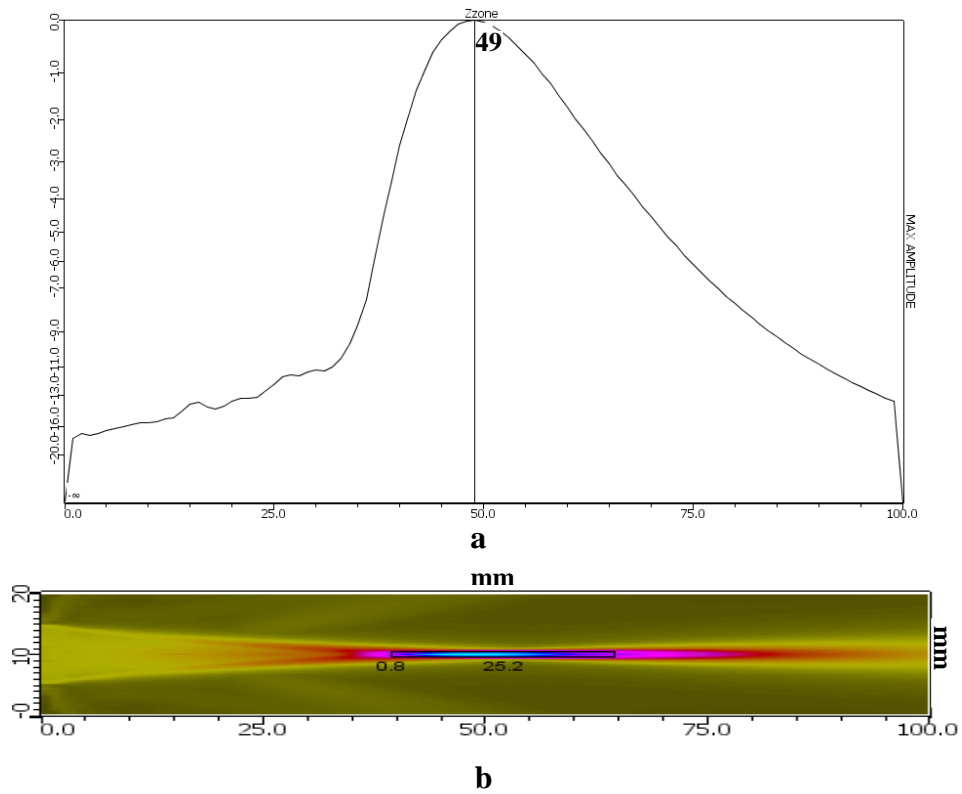


Fig.3.6. The distribution of the amplitude (a) and field (b) along focused transducer's axis

3.2 Investigation of ultrasonic field of different transducers in CIVA software

The objective of this part of thesis is to investigate ultrasonic fields in the sample using different transducers and compare their characteristics. The inspections were performed from composite and metal sides of the object.

Position of 5 MHz, 10 MHz conventional and 10 MHz focused transducers and their computation zone are shown in **Fig.3.7**. The length between transducers and sample N is the length of near field and in the case of focused transducer is the water path. N for 5 MHz transducer is 84 mm, for 10 MHz is 167 mm. In the case of inspection from composite using 10 MHz focused transducer the water path is 40,27 mm, in the case of inspection from metal side the water path is 23,93 mm according to equation (3.3).

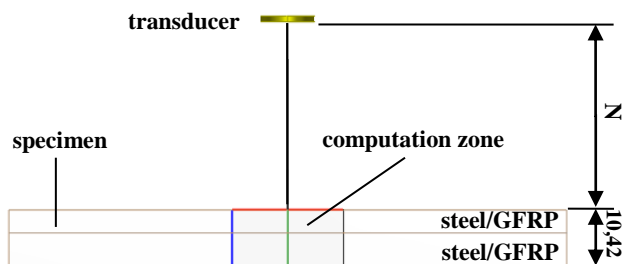


Fig.3.7. Positioning of conventional and focused transducers

The positioning of 3,5 MHz, 5 MHz and 10 MHz phased array transducers are shown in **Fig.3.8**. The inspection using 3,5 MHz and 5 MHz phased array transducers performed with contact method. The Olympus wedge was used for it. The inspection using 10 MHz phased array transducer performed with immersion method. The depth of water is 10 mm. Simple electronic scanning and single point focusing were used for the sample inspection with phased array transducers. Their active aperture is 128 and 64 elements but in scanning only 8 elements. Passive aperture of phased array transducers is 7 mm and the gap between elements is 0,1 mm. In case of 3,5 MHz and 5 MHz phased array transducers element width is 0,9 mm, and in the case of 10 MHz phased array transducer element width is 0,4 mm.

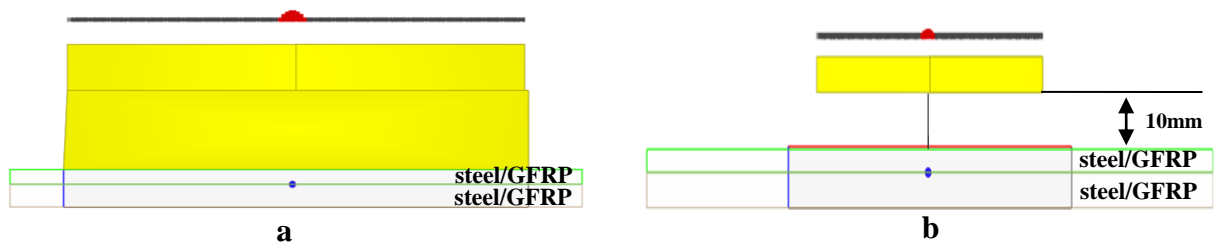


Fig.3.8. Positioning of phased array transducers: a-3,5 MHz and 5 MHz, b-10 MHz

3.2.1 Sample inspection from composite side

First, ultrasonic inspections from composite side were performed. The ultrasonic fields of conventional and focused transducers calculated with 0,1 mm step. The distribution of the field in the sample is shown in **Fig.3.9**.

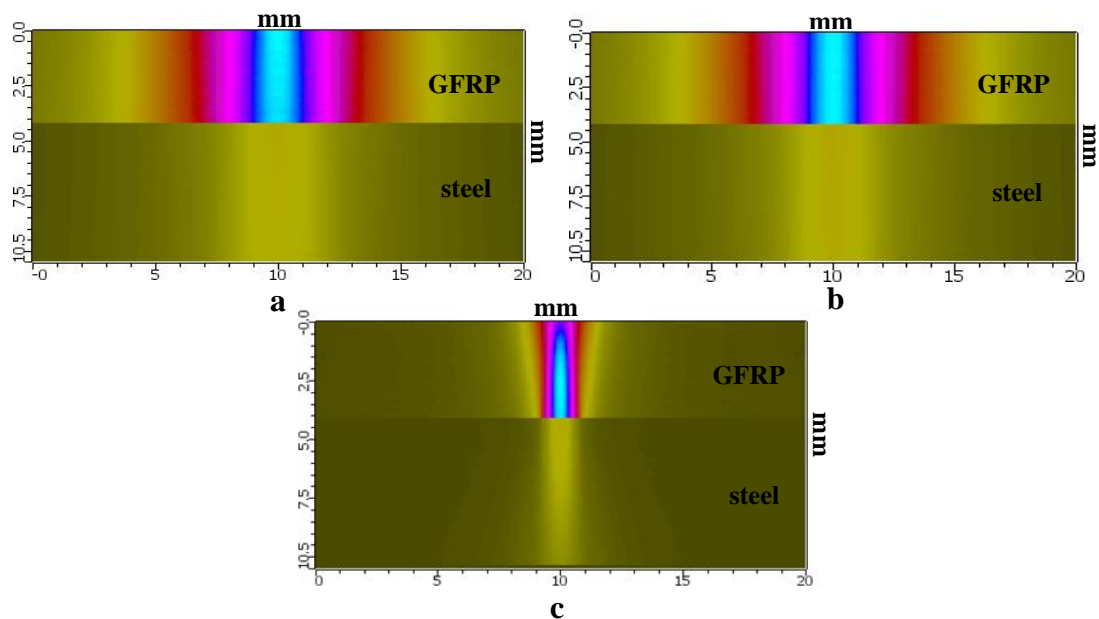


Fig.3.9. Ultrasonic field in the sample: a-5 MHz conventional transducer; b-10 MHz conventional transducer; c-10 MHz focused transducer

Based on results of investigation of ultrasonic fields it can be seen that ultrasonic waves propagates in composite material but only a small part of energy is transmitted to the second media (steel).

The inspections of the sample from composite side with phased array transducers performed as well. The ultrasonic fields of phased array transducers distributed in the sample are shown in **Fig.3.10**.

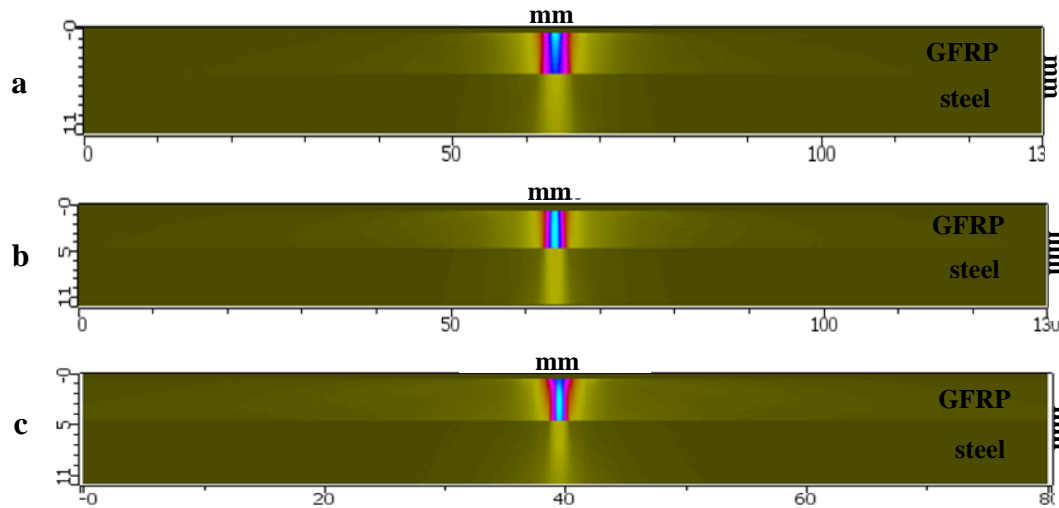


Fig.3.10. Ultrasonic fields of phased array transducers distributed in the sample: a-3,5 MHz, b-5 MHz, c-10 MHz

Based on results of the inspections from composite side, the ultrasonic waves almost don't propagate in metal material as in the case of inspection with conventional transducers. It can be caused due to high attenuation of ultrasonic waves in composite material or great mismatch of acoustic impedances which affects on the percentage of energy that will be reflected at the boundary between 2 media. The reflection coefficients will be calculated to establish the true cause of such propagation of ultrasonic energy in composite and metal materials.

3.2.2 Sample inspection from metal side

Inspections of ultrasonic fields of the sample from metal side were performed. The ultrasonic field distribution in the sample of 5 MHz, 10 MHz and 10 MHz focused transducers are shown in **Fig.3.11**.

Based on results of inspection from metal side with conventional and focused transducers it can be seen that ultrasonic waves propagates in steel and a significant part of energy is transmitted to the second media (GFRP).

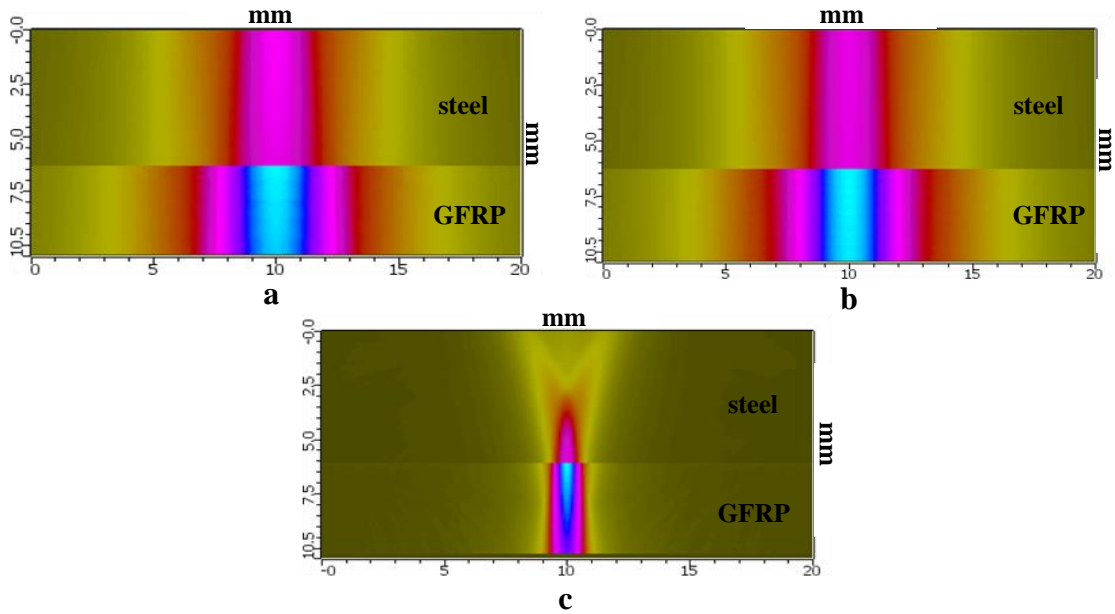


Fig.3.11. Ultrasonic field in the sample: a-5 MHz conventional transducer; b-10 MHz conventional transducer; c-10 MHz focused transducer

The inspections of the sample from metal side with phased array transducers were performed as well. The ultrasonic fields of phased array transducers distributed in the sample are shown in **Fig.3.12.**

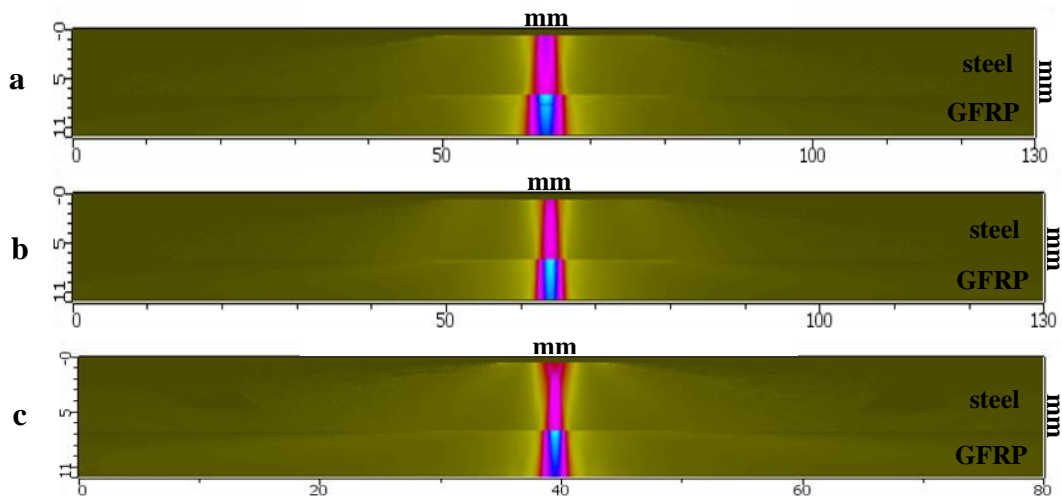


Fig.3.12. Ultrasonic fields of phased array transducers distributed in the sample: a-3,5 MHz, b-5 MHz, c-10 MHz

Based on results of inspection from metal side with phased array transducers it can be seen that ultrasonic waves propagate in steel and a significant part of energy is transmitted to the second media (GFRP). It can be caused due to low attenuation of ultrasonic waves in steel or small mismatch of acoustic impedances which affects on the percentage of energy that will be reflected at the boundary between 2 media. The reflection coefficients will be calculated to

establish the true cause of such propagation of ultrasonic energy in composite and metal materials.

3.3 Estimation of the reflection coefficients

Acoustic impedances of materials describe what part of the ultrasonic waves will be reflected at the boundary between two media, and what part will be transmitted to the second media. Since the values of acoustic impedances of materials on both sides of the boundary are known (Table 2.2) the part of ultrasonic wave which is reflected is calculated according to equation [19]:

$$R = \left(\frac{z_2 - z_1}{z_2 + z_1} \right)^2, \quad (3.3)$$

The reflection coefficient at the boundary between water and composite is 0,36. In other words 36 % of energy is reflected and the rest is transmitted to GFRP. The reflection coefficient at the boundary between water and steel is 0,86 or 86 % of energy is reflected. The reflection coefficient at the boundary between steel and GFRP is 0,58 or 58 % of energy is reflected.

As a result in the case of inspection from composite side 36 % of energy is reflected from the boundary between water and GFRP what is more than 2 times lower comparing to inspection from metal side. That is why the reason of transmission of small part of ultrasound energy from composite to steel is in high attenuation of GFRP.

3.4 Investigation of sample with defects in CIVA software

Using the toolbox of defect interaction of the CIVA program, it is possible to evaluate the response of expected defects in the sample. Different ways of the defect inspection can be compared with regard to detection and sizing capability [21]. In this part of thesis the inspection of defects from both sides of the sample using conventional and phased array transducers were performed. Parameters of the defects are given in **Table 3.2**.

Table 3.2. Parameters of the defects

№	Geometry	Length, mm	Width, mm
1	Rectangular	25	25
2	Rectangular	15	15
3	Rectangular	5	5

The sample and position of delaminations is illustrated in **Fig.3.13**. One layer of the sample is GFRP and the other one is stainless steel.

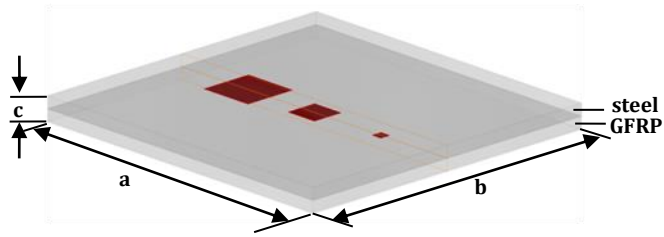


Fig.3.13. Position of the delaminations: a-length, b-width, c-thickness

The experimental set-up of the inspection with conventional transducers is shown in **Fig.3.14.**

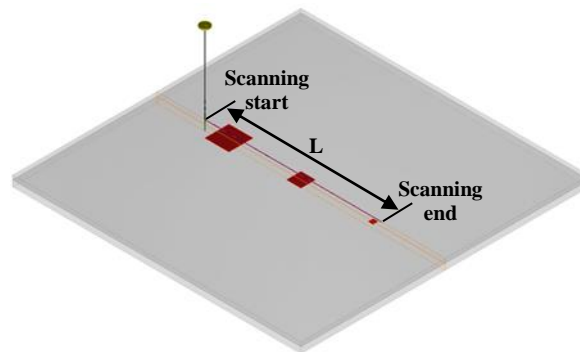


Fig.3.14. Experimental set-up of the inspection with 5 MHz, 10 MHz and 10 MHz focused transducers

The length (L) of mechanical scanning with 5 MHz and 10 MHz transducers is 185 mm, the length of mechanical scanning with 10 MHz focused transducer is 190 mm.

The experimental set-up of the inspection with phased array transducers are shown in **Fig.3.15.**

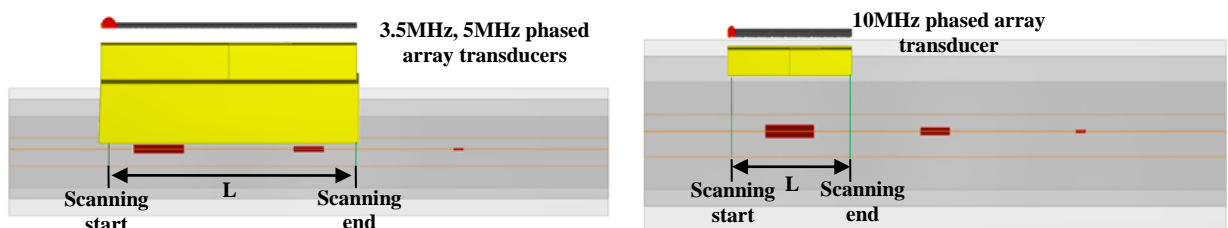


Fig.3.15. Experimental set-up of the inspection with 3,5 MHz, 5 MHz and 10 MHz phased arrays

The incident dimension of 3,5 MHz and 5 MHz phased array transducers is 128 mm and equals to the length (L) of electronic scanning. The incident dimension of 10 MHz phased array transducer is 64 mm and equals to the length (L) of electronic scanning.

3.4.1 Sample inspection from composite side

First, sample of dissimilar material joints was inspected from composite side. The attenuation was taken into account. The B-scan of the inspection with 0,1 mm step of 5 MHz transducer is shown in **Fig.3.16 (a)**. Amplitudes of signals which are reflected from the defect areas (black colour) and from the interface of the sample without defects (red colour) are compared. The A-scans of the sample and 1st delamination are shown in **Fig.3.16 (b)**.

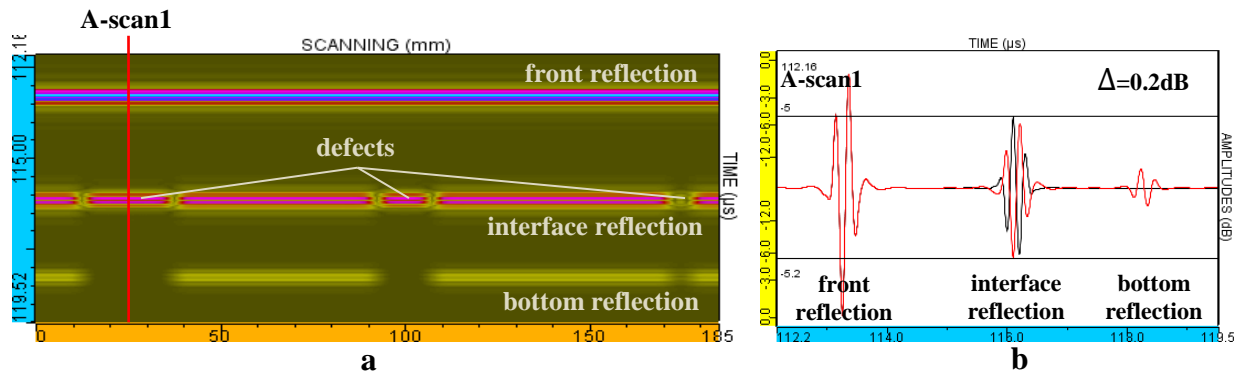


Fig.3.16. B-scan (a) and A-scan (b) of the inspection of the sample with 5 MHz conventional transducer: reflection from the defects-black colour, reflection from the interface-red colour

The B-scan of the inspection with a 0,1 mm step of 10 MHz transducer is shown in **Fig.3.17 (a)**. Amplitudes of signals which are reflected from the defect areas (black colour) and from the interface of the sample without defects (red color) are compared. The A-scans of the sample and 1st delamination are shown in **Fig.3.17 (b)**.

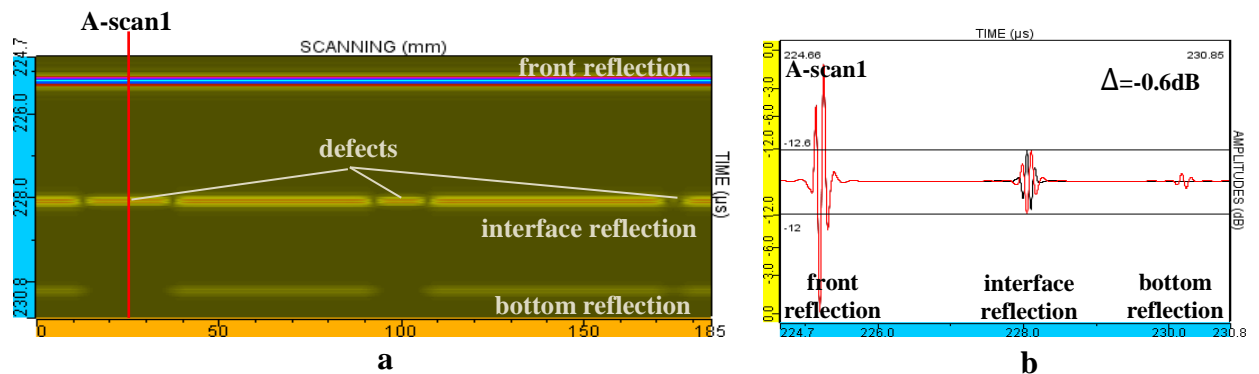


Fig.3.17. B-scan (a) and A-scan (b) of the inspection of the sample with 10 MHz conventional transducer: reflection from the defects-black colour, reflection from the interface-red colour

The B-scan of the inspection with a 0,1 mm step of 10 MHz focused transducer is shown in **Fig.3.18 (a)**. Amplitudes of signals which are reflected from the defect areas (black colour) and from the interface of the sample without defects (red colour) are compared. The A-scans of the sample and 1st delamination are shown in **Fig.3.18 (b)**.

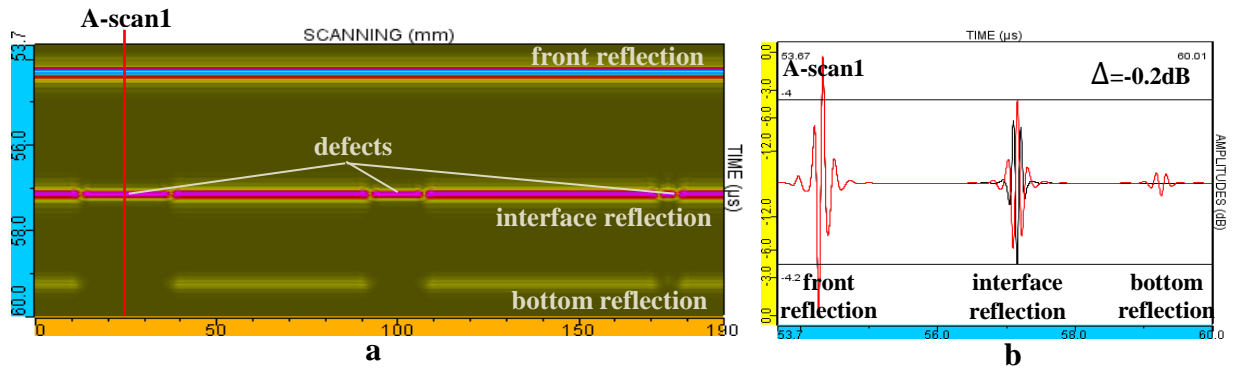


Fig.3.18. B-scan (a) and A-scan (b) of the inspection of the sample with 10 MHz focused transducer: reflection from the defects-black colour, reflection from the interface-red colour

The B-scans of the inspection from composite side with 1 element step of 3,5 MHz phased array transducer are shown in **Fig.3.19 (a, b)**. Amplitudes of signals which are reflected from the defect areas (black colour) and from the interface of the sample without defects (red colour) are compared. The A-scan of the sample and the largest delamination are shown in **Fig.3.19 (c)**.

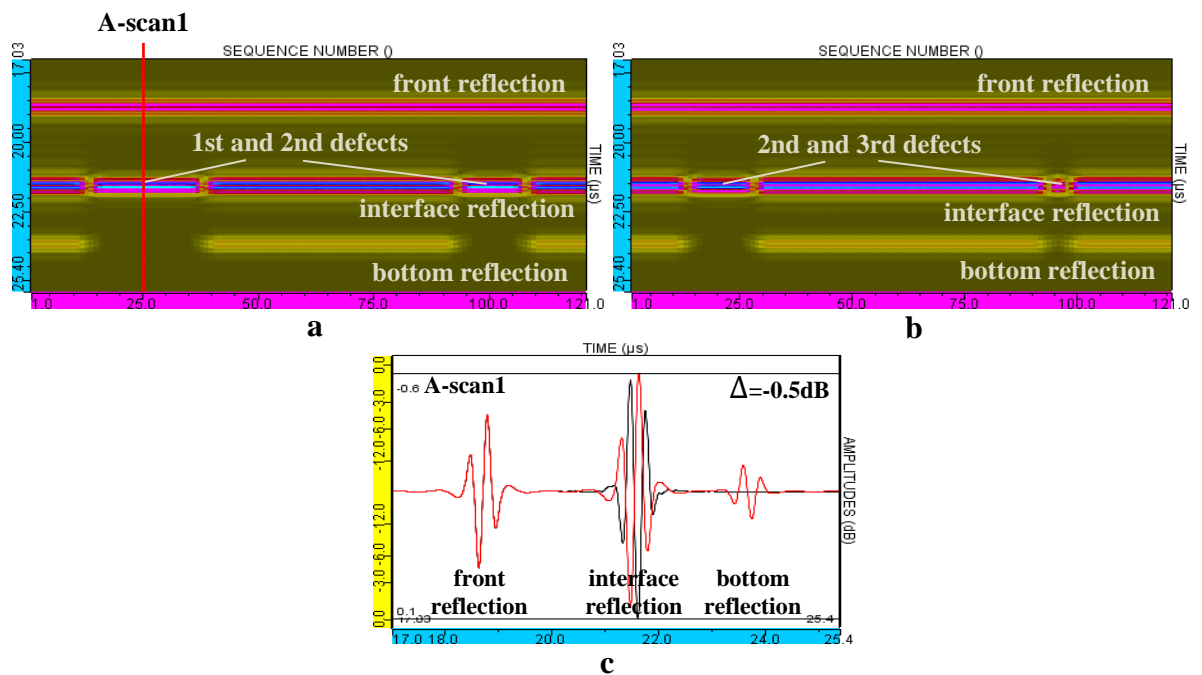


Fig.3.19. B-scans (a-1st and 2nd defects, b-2nd and 3rd defects) and A-scan (c) of the inspection from composite side with 3,5 MHz phased array transducer: black colour-reflection from the defect area, red colour-reflection from the interface

The B-scans of the inspection from composite side with 1 element step of 5 MHz phased array transducer are shown in **Fig.3.20 (a, b)**. Amplitudes of signals which are reflected from the defect areas (black colour) and from the interface of the sample without defects (red colour) are compared. The A-scan of the sample and 1st delamination are shown in **Fig.3.20 (c)**.

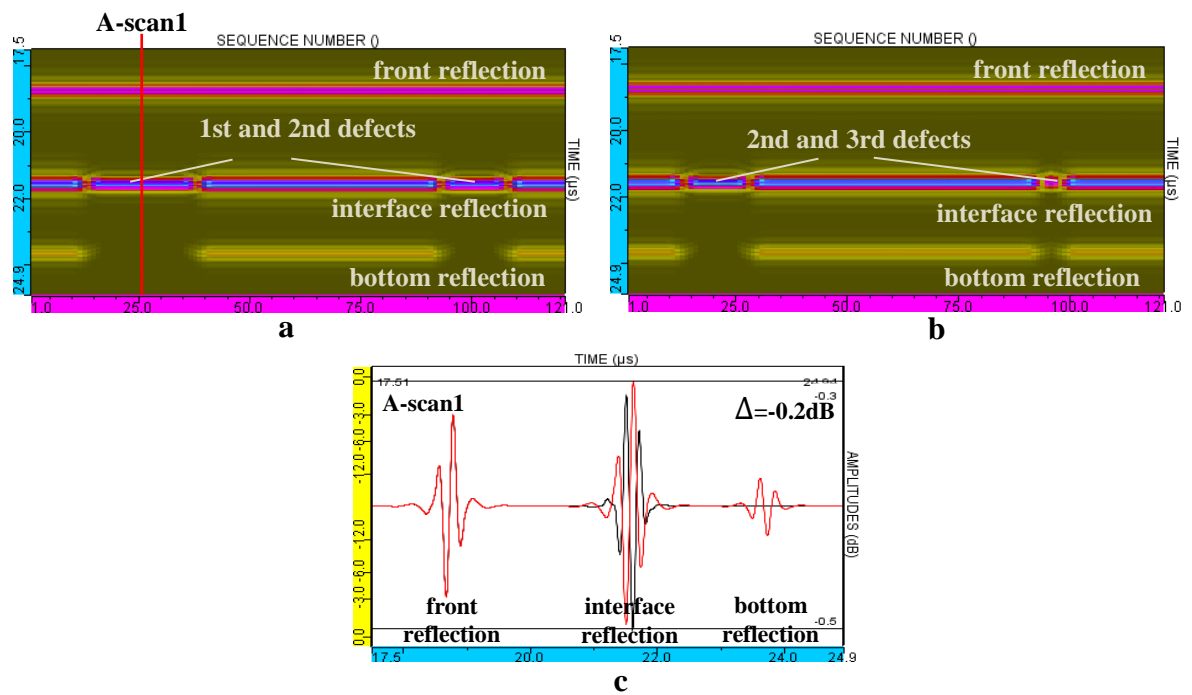


Fig.3.20. B-scans (a-1st and 2nd defects, b-2nd and 3rd defects) and A-scan (c) of the inspection from composite side with 5 MHz phased array transducer: black colour-reflection from the defect area, red colour-reflection from the interface

The B-scans of the inspection from composite side with 1 element step of 10 MHz phased array transducer are shown in **Fig.3.21**. Amplitudes of signals which are reflected from the defect areas (black colour) and from the interface of the sample without defects (red colour) are compared. The A-scan of the sample and 1st delamination are shown in **Fig.3.22**.

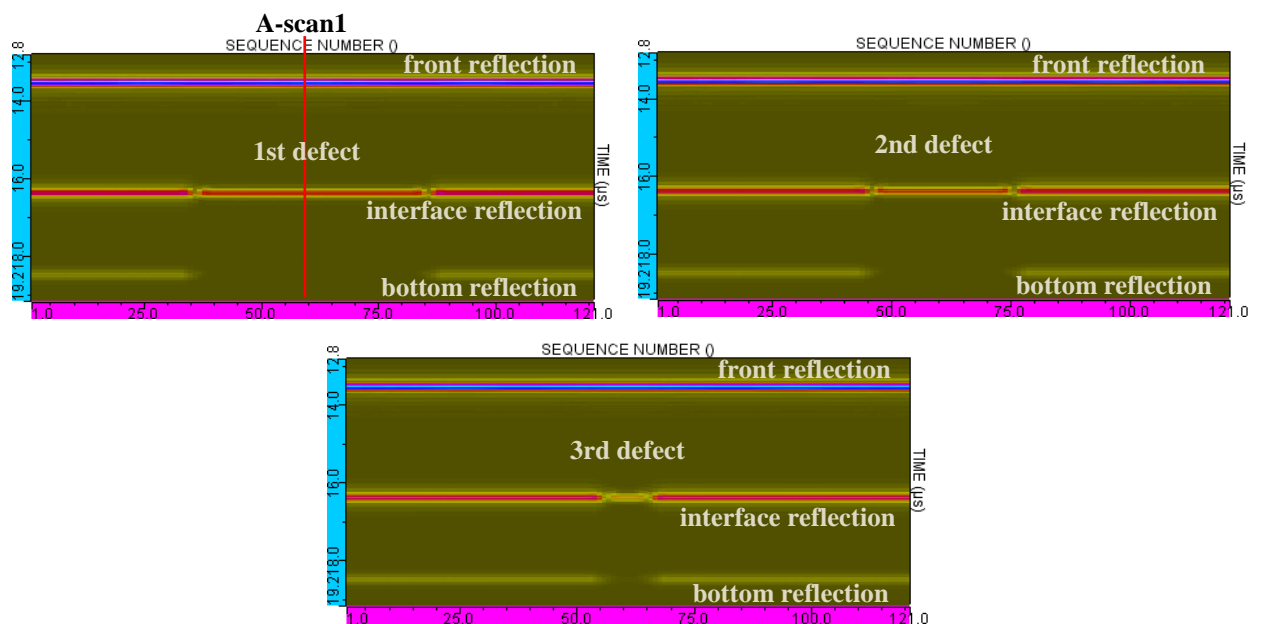


Fig.3.21. B-scans of the inspection from composite side with 10 MHz phased array transducer

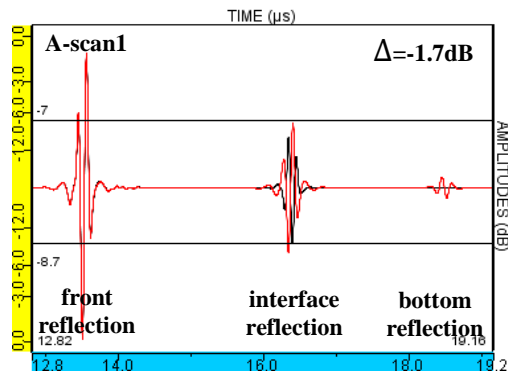


Fig.3.22. A-scan of the inspection from composite side with 10 MHz phased array transducer: black colour-reflection from the defect area, red colour-reflection from the interface.

As a result of inspection from composite side using 10 MHz and 10 MHz focused transducers the signals reflected from 1st defect are 0,6 dB and 0,2 dB weaker than the reflection from the interface. Using 5 MHz conventional transducer the reflection from 1st defect is 0,2 dB stronger than the reflection from interface. In the case of 3,5 MHz, 5 MHz and 10 MHz phased array transducers the signals reflected from 1st defect are 0,2 dB, 0,5 dB and 1,7 dB weaker than the reflection from the interface. Due to small differences in amplitudes it could be difficult to locate the defects in experimental measurements [4].

A-scan signals reflected from 1st defect of all transducers which were used for the inspection in modelling program CIVA are compared. A-scan comparison of 5 MHz, 10 MHz and 10 MHz focused transducers is shown in **Fig.3.23**.

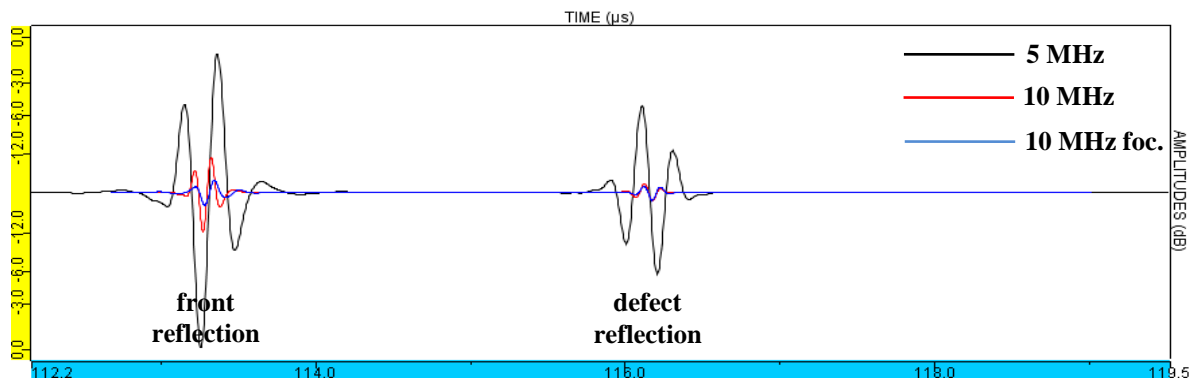


Fig.3.23. A-scan of signals comparison of 5 MHz, 10 MHz and 10 MHz focused transducers

According to A-scan reflection of 5 MHz transducer is 19 dB stronger than reflection of 10 MHz transducer. Reflection of 10 MHz transducer is 4 dB stronger than reflection of 10 MHz focused transducer.

A-scan signals reflected from the largest defect of 3,5 MHz, 5 MHz and 10 MHz phased array transducers which were used for the inspection from composite side in modelling program CIVA are compared. A-scan comparison of transducers is shown in **Fig.3.24**.

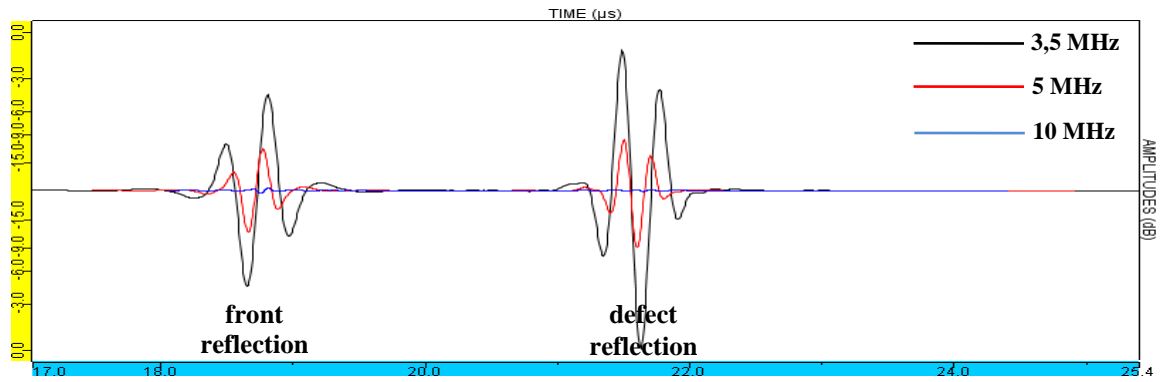


Fig.3.24. A-scan signals comparison of 3,5 MHz, 5 MHz and 10 MHz phased array transducers

In A-scans signal comparison it can be seen that 5 MHz and 3,5 MHz phased array transducers have strongest signal reflections. Reflection of 3,5 MHz phased array is 8,9 dB stronger than 5 MHz phased array reflection. Reflection of 5 MHz phased array is 32,5 dB stronger than reflection of 10 MHz phased array. The lowest amplitude of the signal reflection belongs to 10 MHz phased array transducer.

3.4.2 Sample inspection from metal side

The joint of GFRP and steel was inspected in CIVA software from metal side with conventional and phased array transducers.

The B-scan of the inspection with a 0,1 mm step using 5 MHz transducer is shown in **Fig.3.25.**

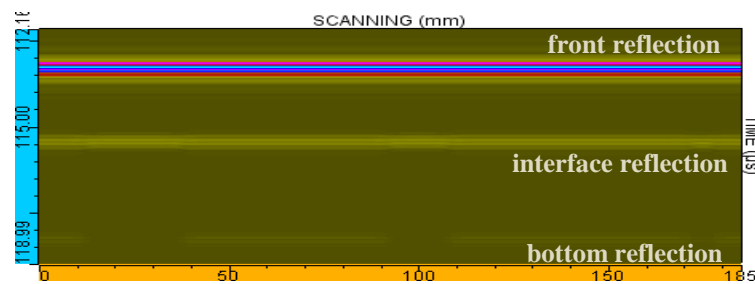


Fig.3.25. B-scan of the inspection of the sample with 5 MHz transducer

Because of the weak signals reflected from the defects and bottom of the sample the visualizations without front reflection were made for all further inspections. The reason of weak reflection in the case of inspection from metal side is in a large value of reflection coefficient at the boundary between water and steel [19]. As it was calculated according to equation (3.3), 86 % of energy is reflected. The B-scan of the inspection with a 0,1 mm step using 5 MHz transducer is shown without front reflection in **Fig.3.26 (a)**. Amplitudes of signals which are

reflected from the defect areas (black colour) and from the interface of the sample without defects (red colour) are compared. The A-scans of the sample and 1st delamination are shown in **Fig.3.26 (b)**.

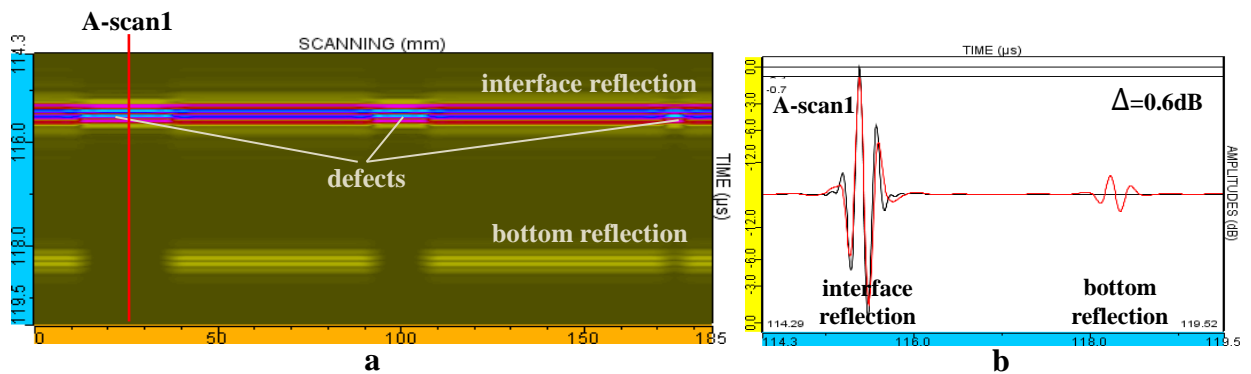


Fig.3.26. B-scan (a) and A-scan (b) of the inspection of the sample with 5 MHz conventional transducer: reflection from the defects-black colour, reflection from the interface-red colour

The B-scan of the inspection with 0,1 mm step using 10 MHz transducer is shown without front reflection in **Fig.3.27 (a)**. Amplitudes of signals which are reflected from the defect areas (black colour) and from the interface of the sample without defects (red colour) are compared. The A-scans of the sample and 1st delamination are shown in **Fig.3.27 (b)**.

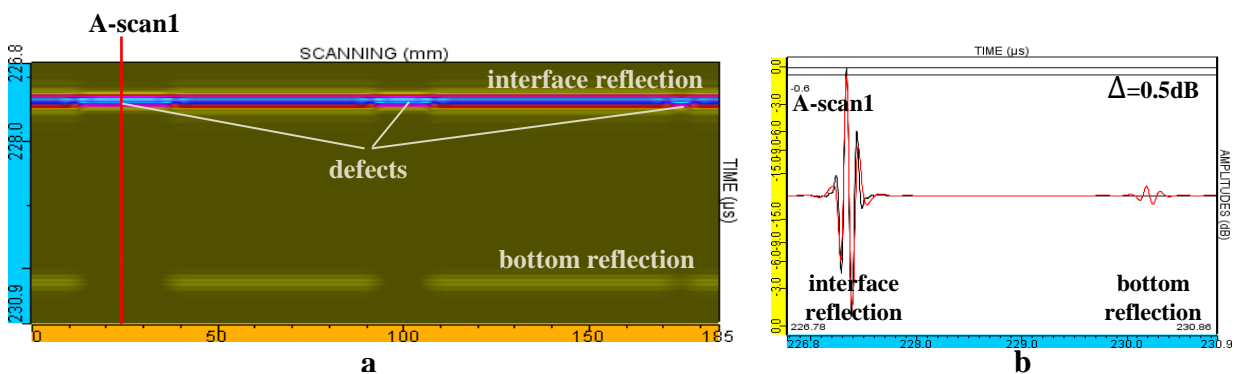


Fig.3.27. B-scan (a) and A-scan (b) of the inspection with 10 MHz conventional transducer: reflection from the defects-black colour, reflection from the interface-red colour

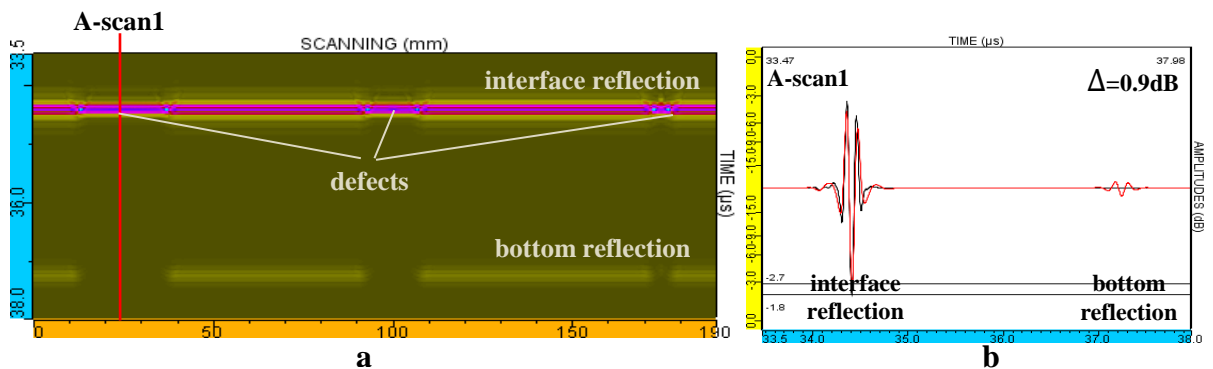


Fig.3.28. B-scan (a) and A-scan (b) of the inspection with 10 MHz focused transducer: reflection from the defects-black colour, reflection from the interface-red colour

The B-scan of the inspection with a 0,1 mm step using 10 MHz focused transducer is shown without front reflection in **Fig.3.28 (a)**. Amplitudes of signals which are reflected from the defect areas (black colour) and from the interface of the sample without defects (red colour) are compared. The A-scans of the sample and 1st delamination are shown in **Fig.3.28 (b)**.

The B-scan of the inspection with a 1 element step using 3,5 MHz phased array transducer is shown without front reflection in **Fig.3.29 (a)**. Amplitudes of signals which are reflected from the defect areas (black colour) and from the interface of the sample without defects (red colour) are compared. The A-scan of the sample and 1st delamination are shown in **Fig.3.29 (b)**.

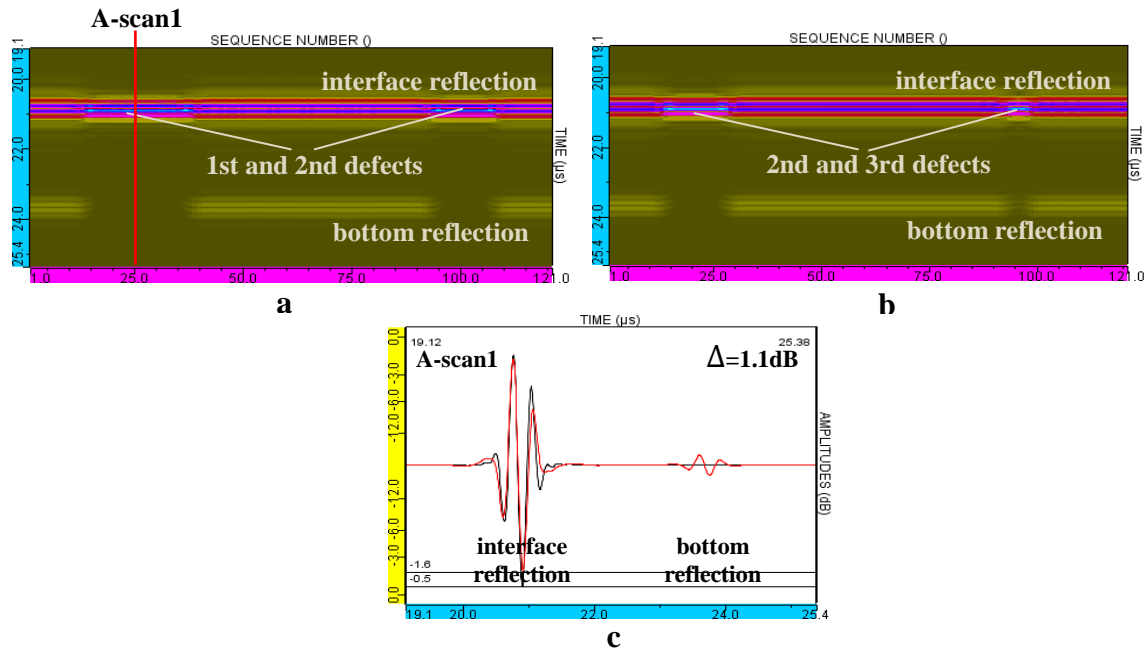


Fig.3.29. B-scans (a-1st and 2nd defects, b-2nd and 3rd defects) and A-scan (c) of the inspection with 3,5 MHz phased array transducer: black colour-reflection from the defect area, red colour-reflection from the interface

The B-scans of the inspection from metal side with 1 element step using 5 MHz phased array transducer are shown without front reflection in **Fig.3.30 (a)**. Amplitudes of signals which are reflected from the defect areas (black colour) and from the interface of the sample without defects (red colour) are compared. The A-scan of the sample and 1st delamination are shown in **Fig.3.30 (b)**.

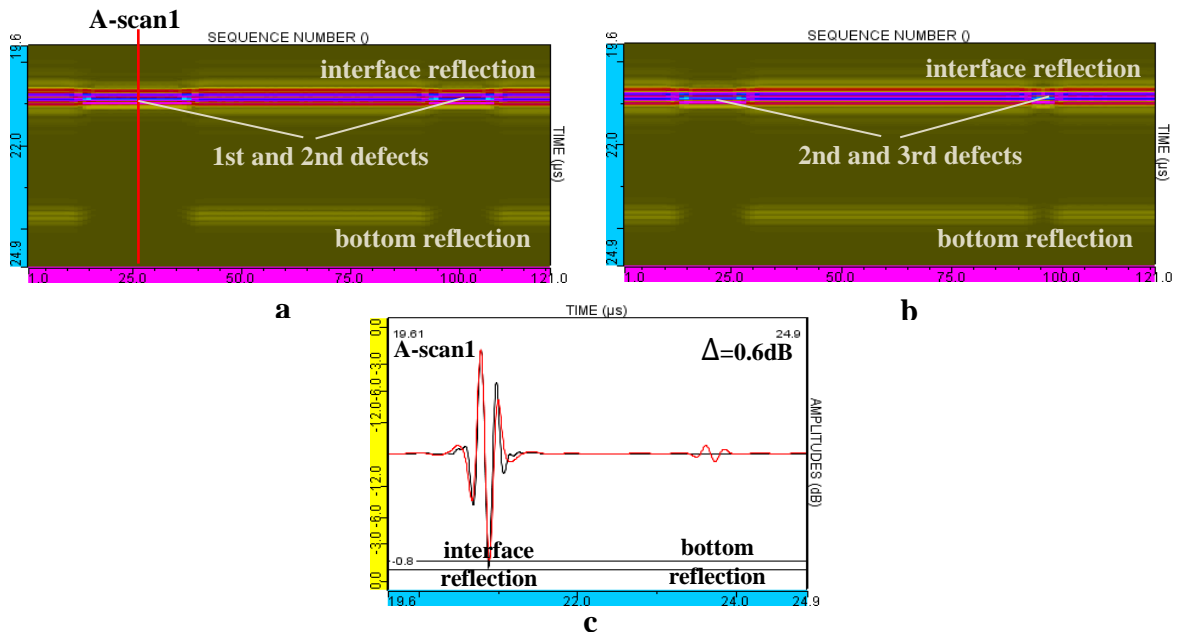


Fig.3.30. B-scans (a-1st and 2nd defects, b-2nd and 3rd defects) and A-scan (c) of the inspection with 5 MHz phased array transducer: black colour-reflection from the defect area, red colour-reflection from the interface

The B-scans of the inspection from metal side with 1 element step using 10 MHz phased array transducer are shown without front reflection in **Fig.3.31**. Amplitudes of signals which are reflected from the defect areas (black colour) and from the interface of the sample without defects (red colour) are compared. The A-scan of the sample and 1st delamination are shown in **Fig.3.32**.



Fig.3.31. B-scans of the inspection from the metal side with 10 MHz phased array transducer

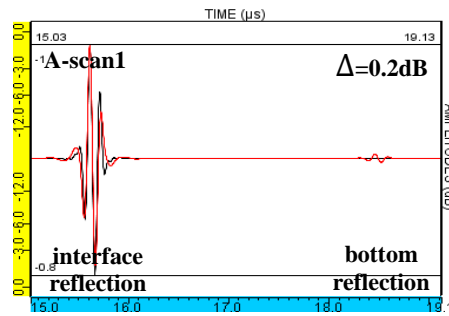


Fig.3.32. A-scan of the inspection from the metal side with 10 MHz phased array transducer:
 black colour-reflection from the defect area, red colour-reflection from the interface

As a result of the inspection from metal side using 5 MHz, 10 MHz and 10 MHz focused transducers the signals reflected from 1st defect are 0,6 dB, 0,5 dB and 0,9 dB stronger than the reflection from the interface. In the case of 3,5 MHz, 5 MHz and 10 MHz phased array transducers the signals reflected from 1st defect are 1,1 dB, 0,6 dB and 0,2 dB stronger than the reflection from the interface. Due to small differences in amplitudes it could be difficult to locate the defects from metal side in experimental measurements as well [4].

A-scan signals reflected from 1st defect of all transducers which were used for the inspection in modelling program CIVA are compared. A-scan comparison of 5 MHz, 10 MHz and 10 MHz focused transducers is shown in **Fig.3.33**.

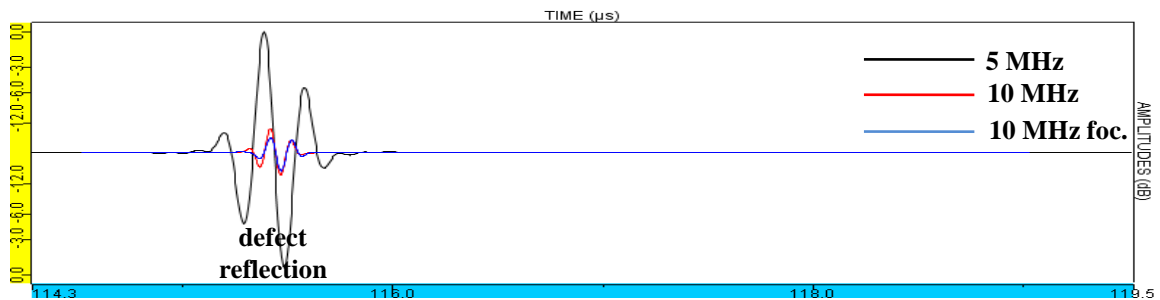


Fig.3.33. A-scan signals comparison of 5 MHz, 10 MHz and 10 MHz focused transducers

According to A-scan, reflection of 5 MHz transducer is 13,9 dB stronger than reflection of 10 MHz transducer. Reflection of 10 MHz transducer is 4,2 dB stronger than reflection from 10 MHz focused transducer.

A-scan signals reflected from the largest defect of 3,5 MHz, 5 MHz and 10 MHz phased array transducers which were used for the inspection from metal side in modeling program CIVA are compared. A-scan comparison of transducers is shown in **Fig.3.34**.

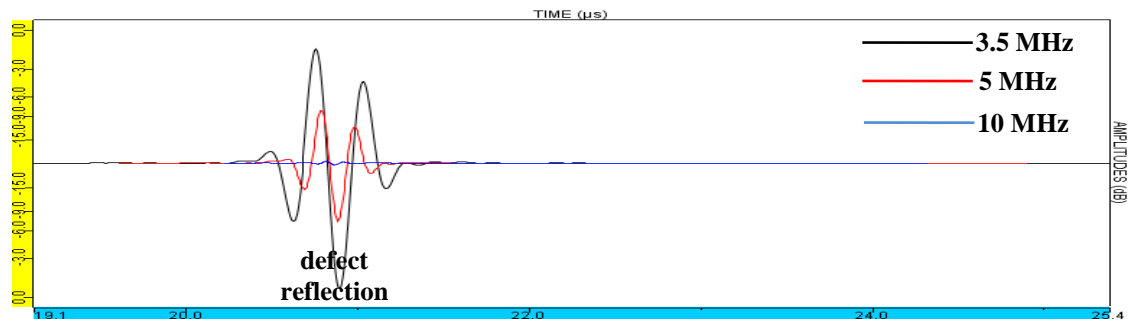


Fig.3.34. A-scan signals comparison of 3,5 MHz, 5 MHz and 10 MHz phased array transducers

In A-scans signal comparison it can be seen that 5 MHz and 3,5 MHz phased array transducers have strongest signal reflections. Reflection of 3,5 MHz phased array is 6,8 dB stronger than 5 MHz phased array reflection. Reflection of 5 MHz phased array is 34,1 dB stronger than reflection of 10 MHz phased array. The lowest amplitude of the signal reflection belongs to 10 MHz phased array transducer.

As a result the strongest reflections from the defect belong to 3,5 MHz and 5 MHz conventional and phased array transducers. Increasing frequency of transducer the attenuation of ultrasound increases as well. Due to it the reflection from the defect can be very low and it will be difficult to distinguish delaminations.

3.5 CIVA investigation of the attenuation influence

The comparison Δ of the amplitudes of the signal reflected from the interface with and without applying attenuation in CIVA software was performed. A-scans of the comparison of attenuations in composite and metal using 5 MHz phased array transducer are shown in **Fig.3.35**.

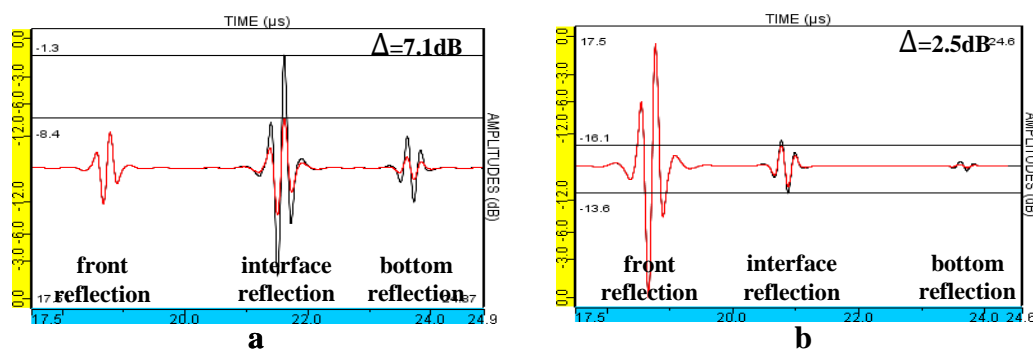


Fig.3.35. A-scans of the comparison of attenuations (black colour-reflection without attenuation, red colour-reflection with attenuation): a-inspection from composite side, b-inspection from metal side

According to results of attenuation comparison the GFRP is almost 3 times more attenuating material than steel.

3.6 Conclusions

According to results of calculation of reflection coefficients R , 86 % of ultrasound energy will be reflected from the boundary between water and steel, and 36 % from the boundary between water and GFRP. The other part of energy transmits to the second media. In spite of this the investigation of ultrasonic fields and attenuation influence shows that GFRP is almost 3 times more attenuating material than steel. Therefore the ultrasonic inspection of dissimilar material joint is selected to be performed from metal side in experimental part.

The defect inspections using conventional and phased array transducers show that the amplitude difference between reflection from the delaminations and reflection from the area of interface without delamination is very low (about 0,1-1,7dB). As a result it could be difficult to locate the defects experimentally [4].

According to amplitude comparisons of interface reflections of all used transducers, the strongest signal belongs to 3,5 MHz and 5 MHz conventional and phased array transducers. The weakest signal belongs to 10 MHz focused and phased array transducers. Increasing the frequency of transducer the attenuation value increases as well. As a result it will be more difficult to locate delaminations using high frequency transducer. 3,5 MHz and 5 MHz phased array transducers are more suitable for the ultrasonic inspection of joint of dissimilar materials and were selected to be used in experimental part [4], [16], [17].

4 EXPERIMENTAL EVALUATIONS

Commonly all kind of materials as metals, plastics, composites, fiberglass, ceramics and others can be measured ultrasonically [7]. In this work the joint of metal and glass fibre reinforced plastics is under inspection. The ultrasound technique and transducers which will be used are selected according to analysis and results of investigation obtained in previous part. In **Table 4.1** acoustic properties of steel and GFRP are presented:

Table 4.1. Theoretical velocities in different materials

Material	Theoretical velocity of longitudinal waves c , m/s	Theoretical velocity of transverse waves c , m/s	Acoustic impedance Z , $M\text{Rayl}$
Steel	5 940	3 251	45,4
GFRP	3 150	1 727	6,04

Dimension of the joint of GFRP and steel is 300*300*10,42 (mm). The thickness of GFRP layer is 4,12 mm and steel layer is 6,30 mm.

4.1 Ultrasonic velocity measurement

Different types of materials transmit ultrasound waves at different speeds. Generally ultrasound speed is faster in hard materials and slower in soft materials. The temperature influences on the speed and can change it significantly. In order the depth of the defects, ultrasound velocity in the investigated materials have to be known [24].

Firstly, the ultrasound velocity in metal is measured and calculated. Used equipment:

- flaw detector *Olympus Omniscan MX*;
- 15 MHz normal incidence longitudinal wave transducer;
- joint of dissimilar materials.

Experimental set-up for measurement of velocity in metal with echo impulse mode is shown in **Fig.4.1**.

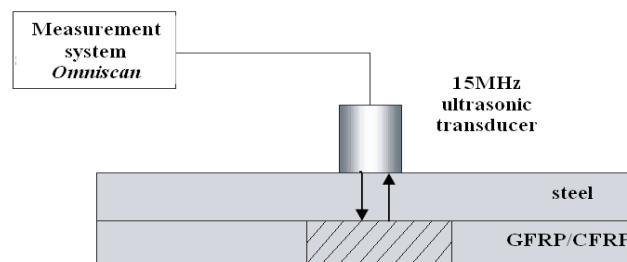


Fig.4.1. Experimental set-up for measurement of velocity in steel [16]

Seven independent measurements performed using 15 MHz transducer without delay line and reflected ultrasound signals from the bottom of metal material registered. Averaged time

interval of the reflected signals and the thickness H of the samples are presented in **Table 4.2**. The ultrasound velocities of longitudinal waves are calculated according to the equation:

$$c = \frac{2H}{\Delta t} \quad (4.1)$$

The time interval between two reflected signals from the bottom of the sample is calculated according to the equation:

$$\Delta t = (t_2 - t_1) \quad (4.2)$$

Where t_2 is a time of second reflected signal and t_1 is a time of first reflected signal [16].

A-scan of one time interval measurement of the reflected signals from the bottom of the sample is shown in **Fig. 4.2**. The initial starting point is at zero crossing.

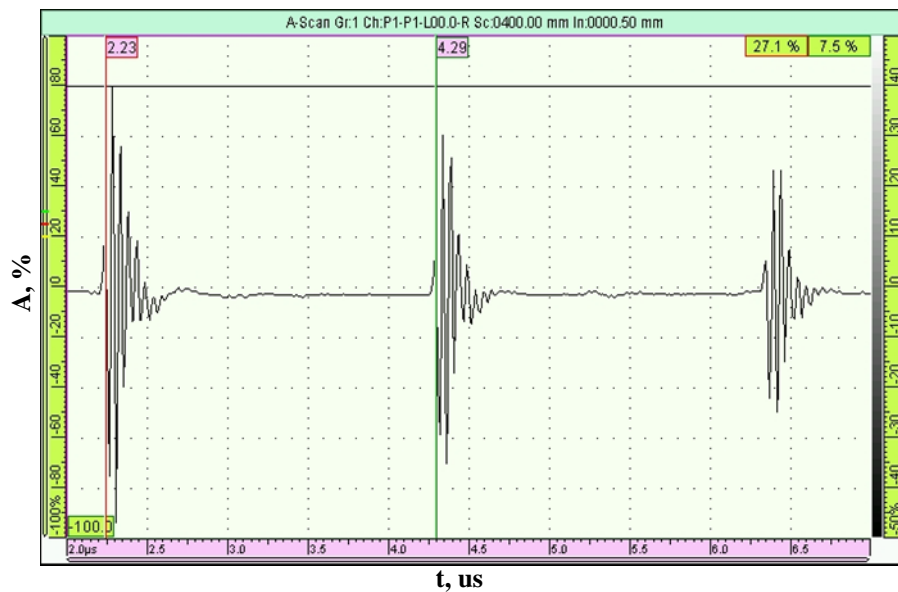


Fig.4.2. A-scan of the reflected signals from bottom of the steel

Table 4.2. Parameters of measurements and calculations

Sample	Thickness H , mm	Averaged time interval Δt , us	Calculated velocity c , m/s
Steel	6,30	2,0571	6 125

It should be noticed that velocity of propagation of ultrasonic waves in composite material (anisotropic elastic material) strongly depends on the angle between the ultrasonic beam and the axis of material symmetry [22].

Equipment used for the measurement of ultrasonic velocity in GFRP:

- ultrasonic measurement system *Ultralab*;
- MatLab software;
- immersion 5 MHz transducer;
- joint of dissimilar materials.

Ultralab measurement system is connected for performing through-transmission method. The set-up of system is illustrated in Fig.4.3.

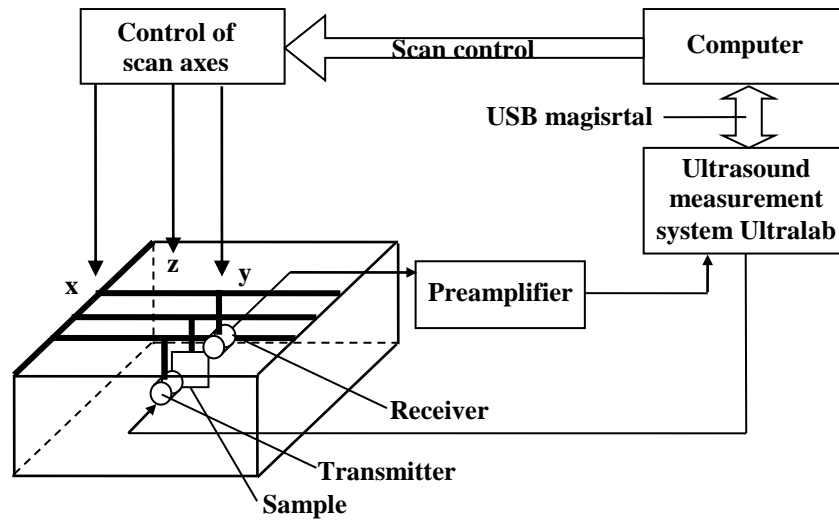


Fig.4.3. The set-up of measurement system [16]

The joint of dissimilar materials and 5 MHz immersion transducer are used for the inspection due to high attenuation in composite material. Through transmission technique is used for this task. The sample is immersed in water and installed on z not moving axis. Firstly, signal was recorded without the sample placed on the way of ultrasound wave propagation, then the sample was placed and signal recorded again. The inspection was performed in the area where steel layer is cut from the sample.

The ultrasound velocity of longitudinal waves is calculated according to the equation:

$$c_{grfp} = \frac{H}{H / c_{water} - (t_1 - t_2)}, \quad (4.3)$$

where H is a thickness of the material, c_{water} is a velocity of ultrasound in water, t_1 is a time of received signal transmitted through the water and t_2 is a time of received signal transmitted through the water and sample [16]. The temperature of the water was 21⁰ C, therefore the value of ultrasound velocity in the water was taken from the table of Lawrence C. Lynnworth.

A-scans of the reflected signals from the GFRP bottom are shown in Fig.4.4. The initial starting point is at zero cross. Time interval of the reflected signals and the thickness H of the samples are presented in Table 4.3.

Table 4.3. Parameters of measurements and calculations

Sample	Thickness H, mm	Time interval between two reflected signals $\Delta t, us$	Calculated velocity $c, m/s$	Ultrasound velocity c in water at 21 ⁰ C, m/s
GFRP	4,12	(53,9-52,54)=1,36	2 914	1 485,372

As a result the ultrasound velocity in steel is about two times higher than in glass fibre reinforced plastic. GFRP is more attenuating material which requires high penetration transducers with transmitter/receivers optimized for operation at low frequencies [24].

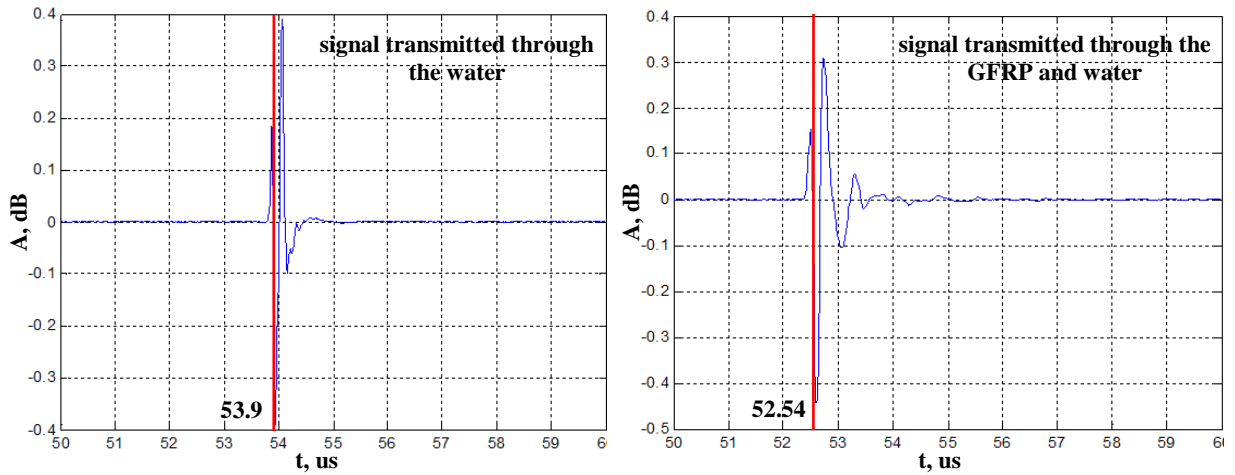


Fig.4.4. A-scan of received signals transmitted through the water and GFRP

4.2 Parameters and characteristics of the inspection of defects with phased array transducers

There are 3 interfacial delaminations between the steel and the composite material. The delaminations were created by PE (polyethylene) tape then spreading a bit of oil over the top of the plate to prevent the epoxy from bonding.

Used equipment for the inspection of joint of dissimilar material:

- flaw detector *Olympus Omniscan MX*;
- 5 MHz linear phased array transducer (5L128-128x7-NW3-P-2.5-OM);
- 3,5 MHz linear phased array transducer (3.5L64-64x7-NW1-P-2.5-OM);
- 0° plastic wedges (SNW3-0L-IHC-C and SNW1-0L-WP5).

The parameters of phased array transducers and wedges were entered in settings of the Omniscan measurement system as well as the parameters of scanning. Data of transducers and wedges are shown in **Table 4.4** and **Table 4.5** respectively.

Table 4.4. Parameters of phased array transducers

Transducer type	Frequency f, MHz	Number of elements	Pitch, mm	Active length, mm	Active elevation, mm	Transducer dimensions, mm		
						L	W	H
Linear	5	128	1	128	7	130	21	35
Linear	3,5	64	1	64	7	66	19	25

Table 4.5. Characteristics of the wedges

Wedge	Nominal Refracted Beam Angle (in Steel)	Probe Orientation	Wedge Dimensions, mm		
			L	W	H
SNW3-0L-IHC-C	0°LW	Normal	130	32	20
SNW1-0L-WP5	0°LW	Normal	66	32	20

Characteristics of scanning with phased array transducers are presented in **Table 4.6.**

Table 4.6. Parameters of scanning with linear phased array transducers

Frequency f , MHz	Transmission type	A_v -virtual aperture, elements	Element step	First element	Last element	Focus depth, mm
5	Focusing	8	1	1	128	6,30
3,5	Focusing	8	1	1	64	6,30

The wavelengths of ultrasound signal in steel are calculated according to equation (4.4) and presented in **Table 4.7.**

Table 4.7. Parameters of scanning with 5 MHz and 3,5 MHz linear phased array transducers

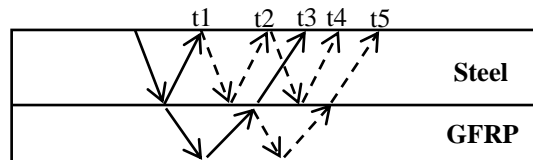
Sample	Wavelength λ , mm	Velocity c , m/s	Frequency f , MHz
Steel	1,225	6 125	5
Steel	1,750	6 125	3,5

$$\lambda = \frac{c}{f} \quad (4.4)$$

Theoretical values of time of ultrasonic wave propagation in the joints of dissimilar materials are calculated according to the equation [24]:

$$t = \frac{2h}{c} \quad (4.5)$$

The structure of wave propagation in layers of the sample is shown in **Fig.4.5.** In **Table 4.8** values of propagation time are presented.

**Fig.4.5.** Wave propagation in the sample**Table 4.8.** Theoretical values of time of ultrasonic wave propagation in the sample

Sample	Thickness h , mm		Velocity c , m/s		$t_{1,us}$	$t_{2,us}$	$t_{3,us}$	$t_{4,us}$	$t_{5,us}$
	Steel	GFRP	Steel	GFRP					
Steel	6,30	4,12	6 125	2 914	2,06	4,11	4,89	6,17	7,72

4.3 Defect inspection of the joint of steel and GFRP with 5 MHz phased array transducer

The Omniscan measurement system was used for the defect inspection and all parameters of transducer were entered. Electronic scanning with 1 element step was performed. Special gel was used as a coupling media. Experimental set-up of defect evaluation from metal side with echo impulse mode is shown in **Fig.4.6**.

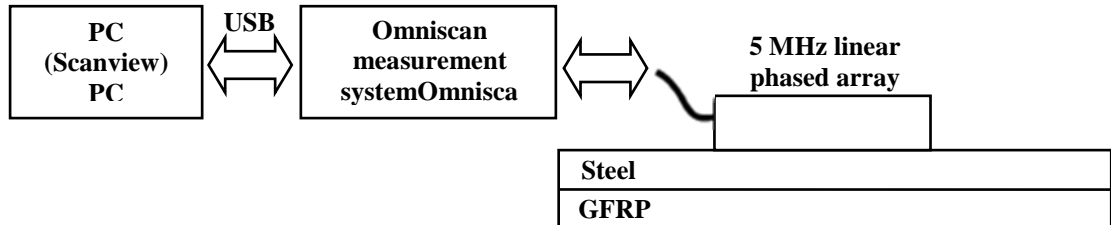


Fig.4.6. Experimental set-up of ultrasonic inspection from metal side [16]

In **Fig.4.7** the set-ups of defect inspection of sample with 5 MHz phased array transducer are shown. The signal was gained to 10 dB and the S-scans of delaminations are shown in **Fig.4.8**.



Fig.4.7. Experimental set-ups of defect evaluation in joint of steel and GFRP: a-inspection of 1st and 2nd delaminations, b- inspection of 2nd and 1st delaminations

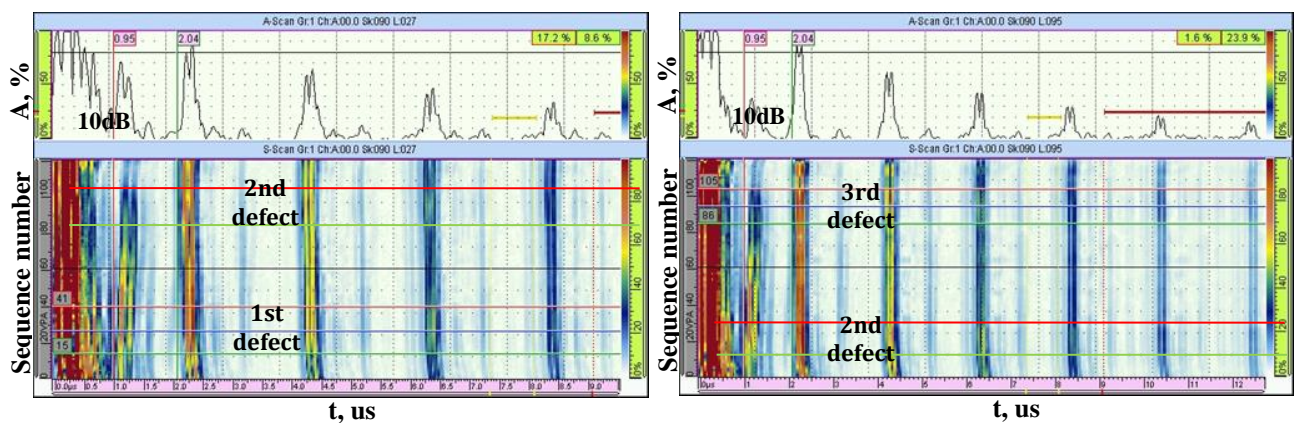


Fig.4.8. S-scans of the inspection of delaminations in steel/GFRP sample with 5 MHz phased array transducer

According to S-scans it can be seen that reflection from the interface of the sample starts at time of 2,04 us what coincides with theoretical calculations and repeats in same time. The value is approximated because signal amplification affects the values of the obtained results on S-scan. The amplitude difference between reflections from the interface and reflections from delaminations can be distinguished due to colour scale. The areas of delaminations have higher amplitude comparing to areas without defects [24], [25].

The signal was gained to 20 dB to see better amplitude contrast of interface and defects The S-scans of delaminations of steel to GFRP sample is shown in **Fig.4.9**.

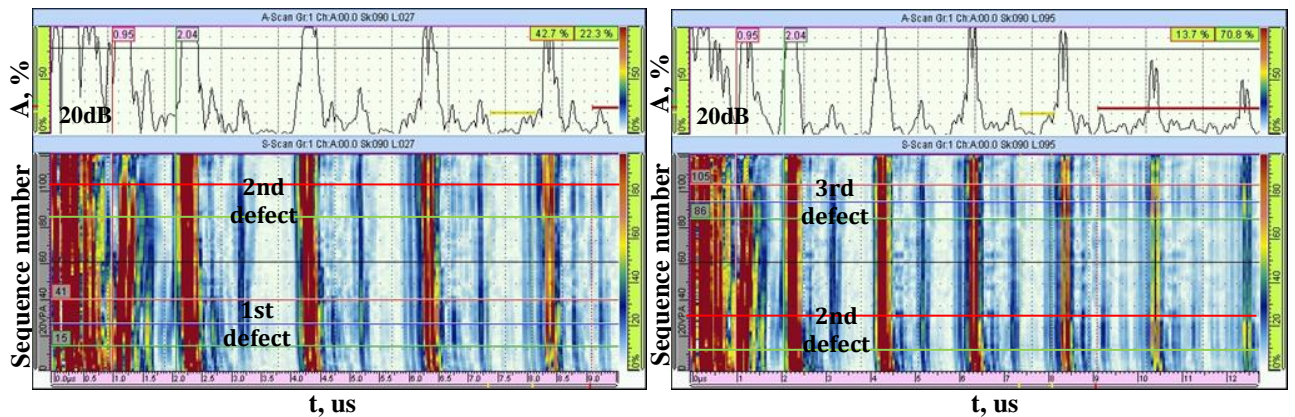


Fig.4.9. S-scan of the inspection of delaminations in steel/GFRP sample with 5MHz phased array transducer

For the exact values of lengths of delaminations the inspection with scales of mm is performed. In **Fig.4.10** the set-ups of defect inspection of the sample with 5 MHz phased array transducer are shown.

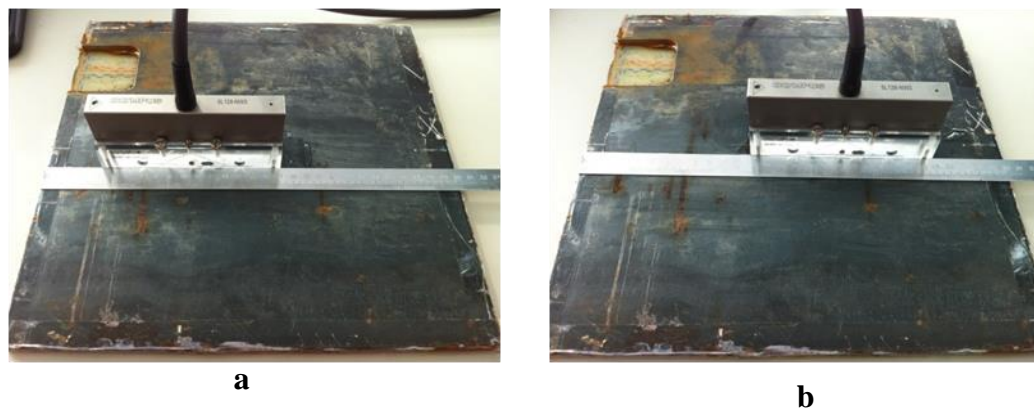


Fig.4.10. Experimental set-ups of defect evaluation in joint of steel and GFRP: a-inspection of 1st and 2nd delaminations, b- inspection of 2nd and 1st delaminations

The signal was gained to 10 dB and the S-scans with a scale of mm are shown in **Fig.4.11**. Further, the signal was gained to 20 dB to see better amplitude contrast of interface and defects and S-scans of delaminations of joint of dissimilar materials are shown in **Fig.4.12**.

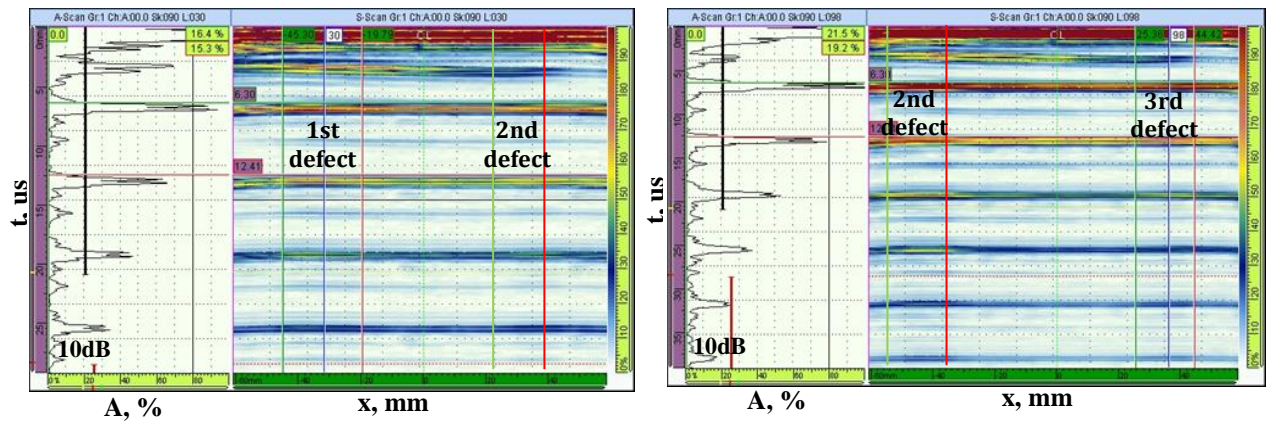


Fig.4.11. S-scan of the inspection of delaminations in steel/GFRP sample with 5 MHz phased array transducer

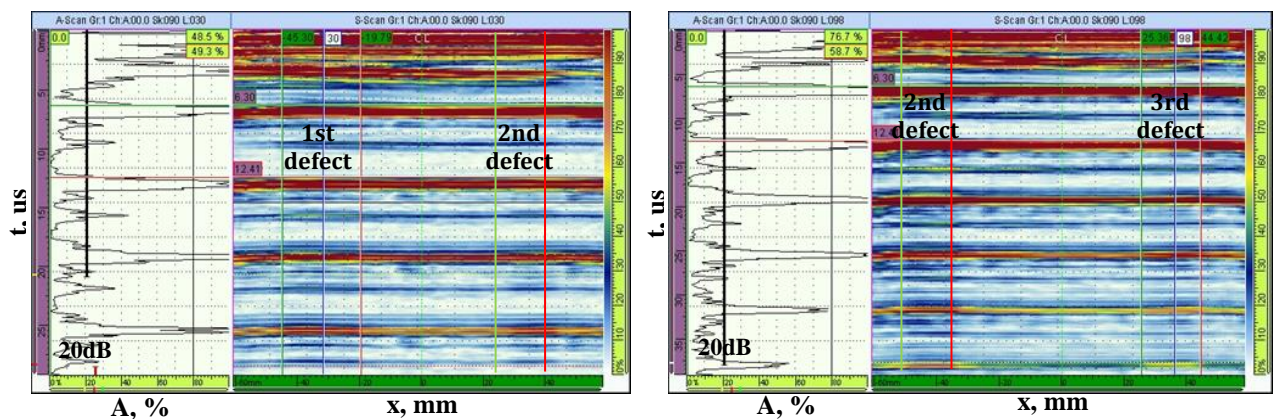


Fig.4.12. S-scan of the inspection of delaminations in steel/GFRP sample with 5 MHz phased array transducer

According to S-scans it can be seen that reflection from the interface of the sample is at the depth of 6,30 mm what coincides with theoretical calculations and repeats approximately in same value. The value is approximated because signal amplification affects the values of the obtained results on S-scan. The amplitude difference between reflections from the interface and reflections from delaminations can be distinguished due to colour scale. The areas of delaminations have higher amplitude comparing to areas without defects [24], [25].

As a result time of flight to each delamination of the object and back to transducer τ_{tofd} was measured independently on A-scan with initial point at zero crossing seven times [16]. In addition seven measurements of length of each delamination were obtained as well. The mean value of these parameters of time of flight and lengths calculated and characterized as more accurate values. The mean value of time of flight to 1st delamination of the object and back to transducer τ_{tofd} is 2,0286 us, to 2nd delamination is 2,0428 us and to 3rd delamination is 2,0429 us. The average value of length of 1st delamination is 25,53 mm, of 2nd delamination is 15,22 mm and of 3rd delamination is 19,59 mm.

The reason of small difference between amplitudes of signal reflection from delaminations and signal reflection from good area of interface is in nearly equal values of reflection coefficients. Therefore the signal had to be gained to find delaminations [19], [24].

4.4 Defect inspection of the joint of steel and GFRP with 3,5 MHz phased array transducer

The Omniscan measurement system was used and all parameters of the transducer were entered. Electronic scanning with 1 element step was performed. Special gel was used as a coupling media. Experimental set-up of defect evaluation from metal side with echo impulse mode is shown in **Fig.4.13**.

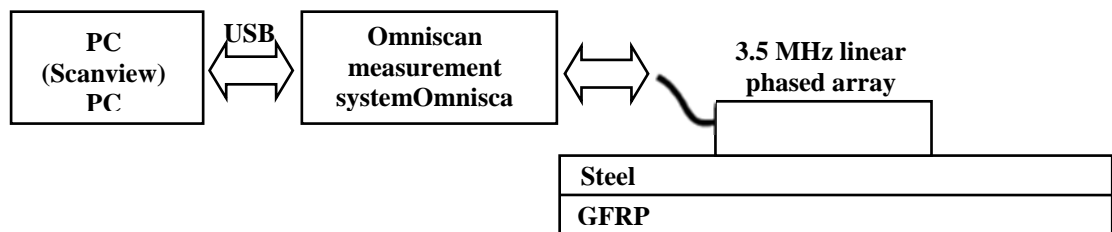


Fig.4.13. Set-up of ultrasonic inspection from metal side with 3,5 MHz transducer [16]

In **Fig.4.14** the set-ups of delamination inspection of the joint of steel and GFRP with 3,5 MHz phased array transducer are shown.

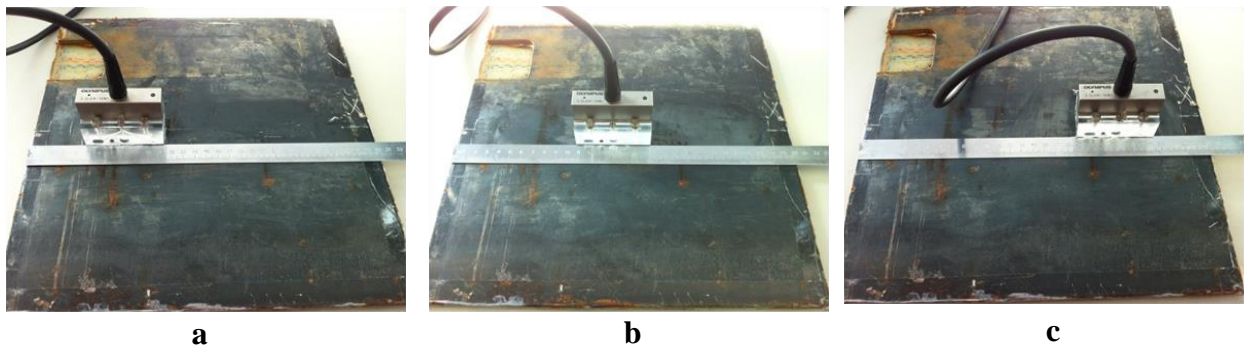


Fig.4.14. Experimental set-ups of defect evaluation in joint of steel and GFRP: a-inspection of 1st delamination, b-inspection of 2nd delamination, c-inspection of 3rd delamination

The signal was gained to 10 dB and the S-scans of delaminations of joint of steel and GFRP are shown in **Fig.4.15**.

According to S-scans it can be seen that reflection from the interface of the sample starts at time of 2,29 us what coincides with theoretical calculations and repeats in same time. The value is approximated because signal amplification affects the values of the obtained results on S-scan. The amplitude difference between reflections from the interface and reflections from delaminations can be distinguished due to colour scale. The areas of delaminations have higher amplitude comparing to areas without defects [24], [25].

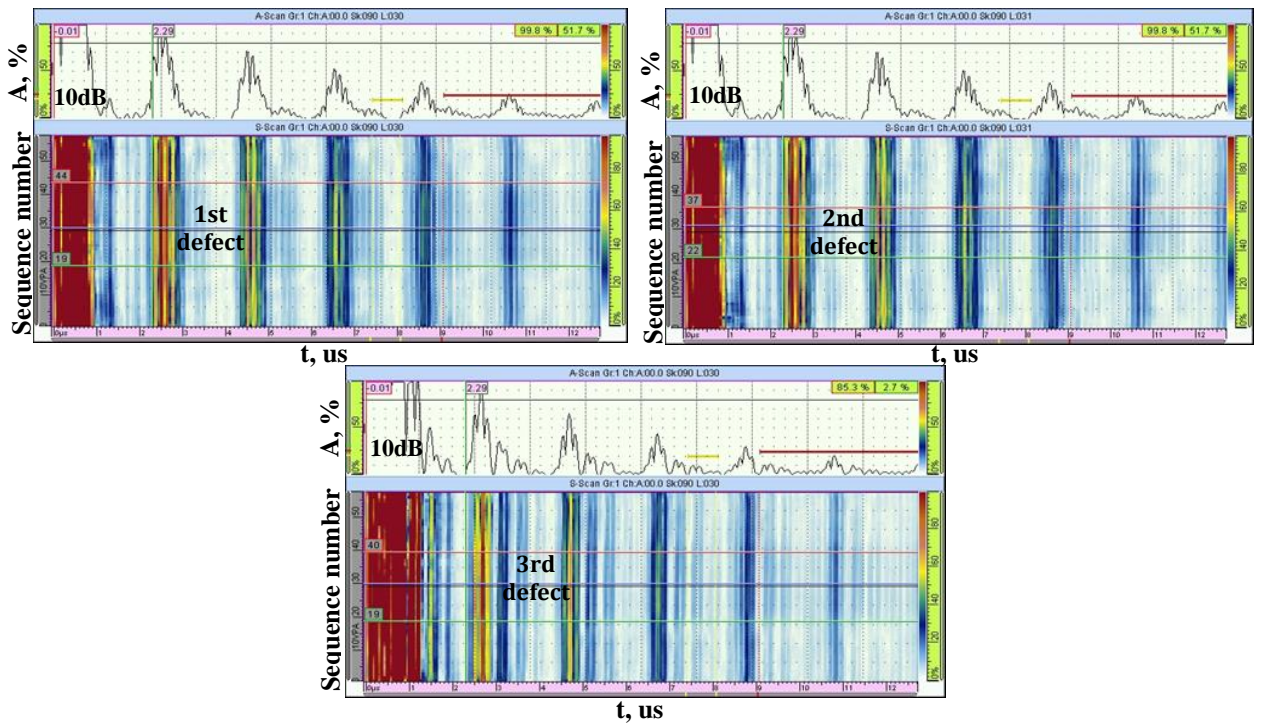


Fig.4.15. S-scan of the inspection of delaminations in steel/GFRP sample with 3,5 MHz phased array transducer

The signal was gained to 20 dB to see better amplitude contrast of interface and defects. The S-scans of delaminations of steel to GFRP sample is shown in **Fig.4.16**.

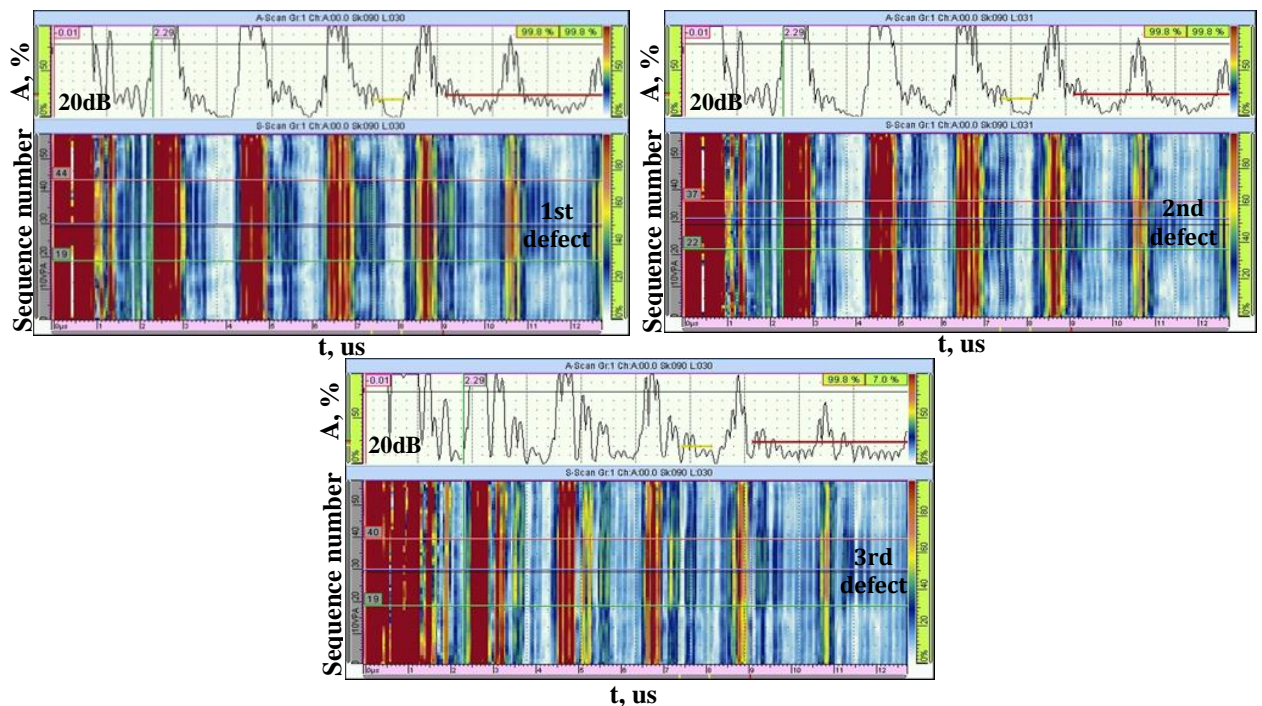


Fig.4.16. S-scan of the inspection of delaminations in steel/GFRP sample with 3,5 MHz phased array transducer

For the exact values of lengths of delaminations the inspection with scales of mm is performed. The signal was gained to 10 dB and the S-scans with a scale of mm are shown in **Fig.4.17**.

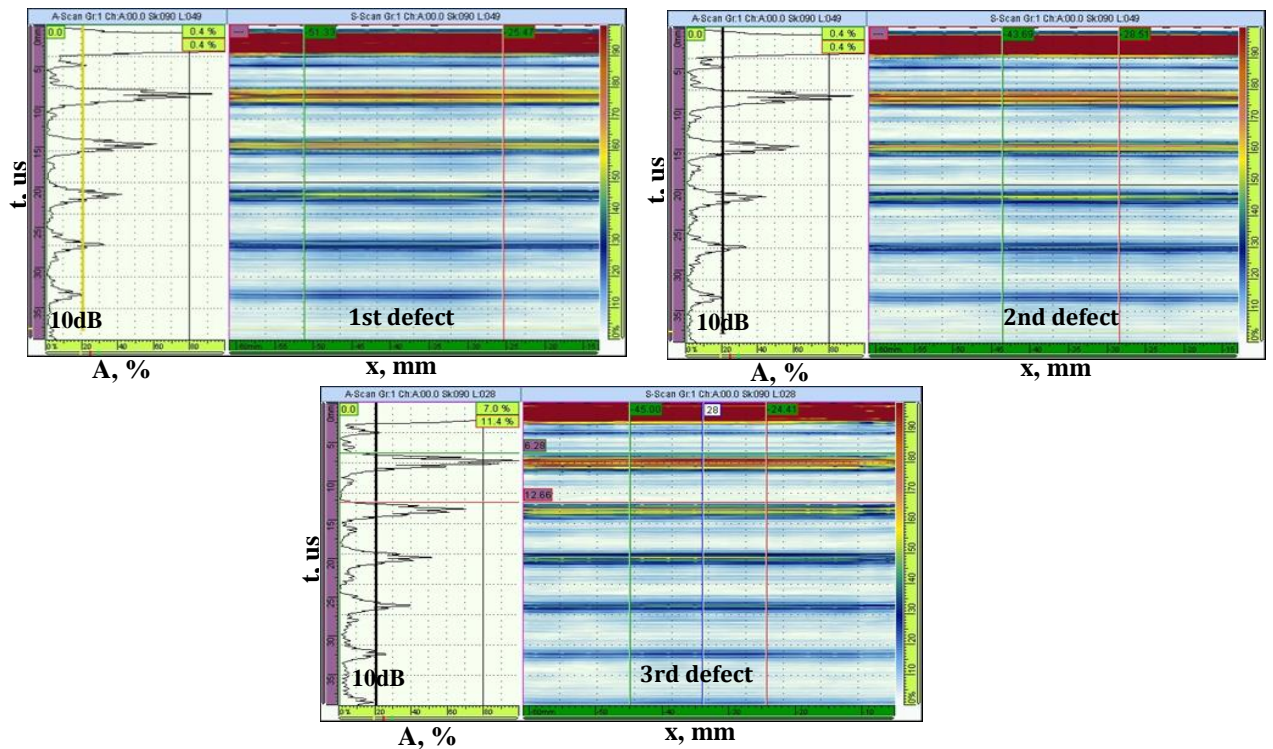


Fig.4.17. S-scan of the inspection of delaminations in steel/GFRP sample with 3,5 MHz phased array transducer

Further, the signal was gained to 20 dB to see better amplitude contrast of interface and defects and S-scans of delaminations of joint of dissimilar materials are shown in **Fig.4.18**.

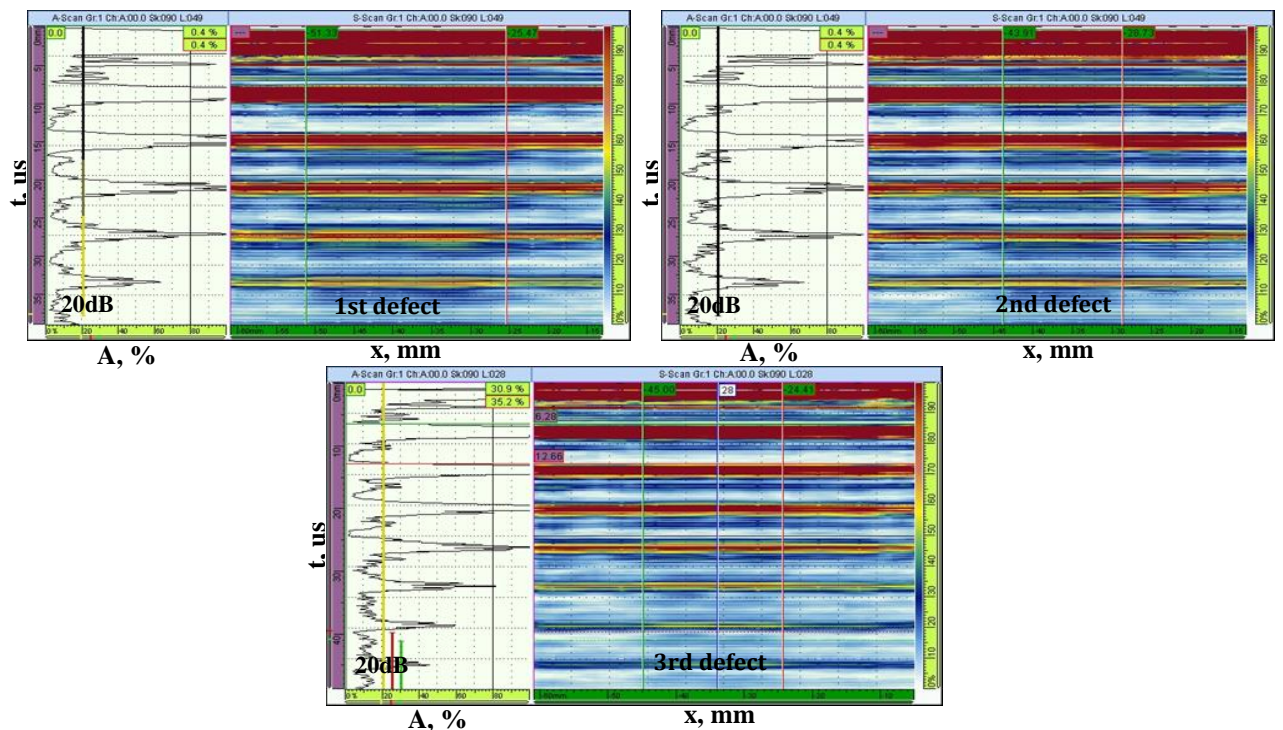


Fig.4.18. S-scan of the inspection of delaminations in steel/GFRP sample with 3,5 MHz phased array transducer

According to S-scans it can be seen that reflection from the interface of the sample is at the depth of 6,28 mm what coincides with theoretical calculations and repeats approximately in same value. The value is approximated because signal amplification affects the values of the obtained results on S-scan. The amplitude difference between reflections from the interface and reflections from delaminations can be distinguished due to colour scale. The areas of delaminations have higher amplitude comparing to areas without defects.

As a result time of flight to each delamination of the object and back to transducer τ_{tof_d} was measured independently on A-scan with initial point at zero crossing seven times [16]. In addition seven measurements of length of each delamination were obtained as well. The mean value of these parameters of time of flight and lengths calculated and characterized as more accurate values. The mean value of time of flight to 1st delamination of the object and back to transducer τ_{tof_d} is 2,0386 us, to 2nd delamination is 2,0414 us and to 3rd delamination is 2,0414 us. The average value of length of 1st delamination is 25,62 mm, of 2nd delamination is 15,24 mm and of 3rd delamination is 20,43 mm.

The reason of small difference between amplitudes of signal reflection from delaminations and signal reflection from good area of interface is in nearly equal values of reflection coefficients. Therefore the signal had to be gained to find delaminations [19], [24].

4.5 Sample inspection using through-transmission method

Through-transmission technique was performed to get a two dimensional presentation, in which position of all delaminations can be observed from the top view.

For the implementation the trough transmission method 2 probes of 5 MHz conventional and 10 MHz focused transducers were used. The transmitting and receiving probes were immersed in the water and aligned [4], [26]. Equipment used for the inspection:

- ultrasonic measurement system *Tecscan*;
- MatLab software;
- immersion 5 MHz conventional and 10 MHz focused transmitting and receiving probes;
- tank with water
- joint of dissimilar materials.

Tecscan measurement system is connected for performing through-transmission method. The whole area of sample was scanned in the axis y and axis z with the step of 0,5 mm. The set-up of system is illustrated in **Fig.4.19**.

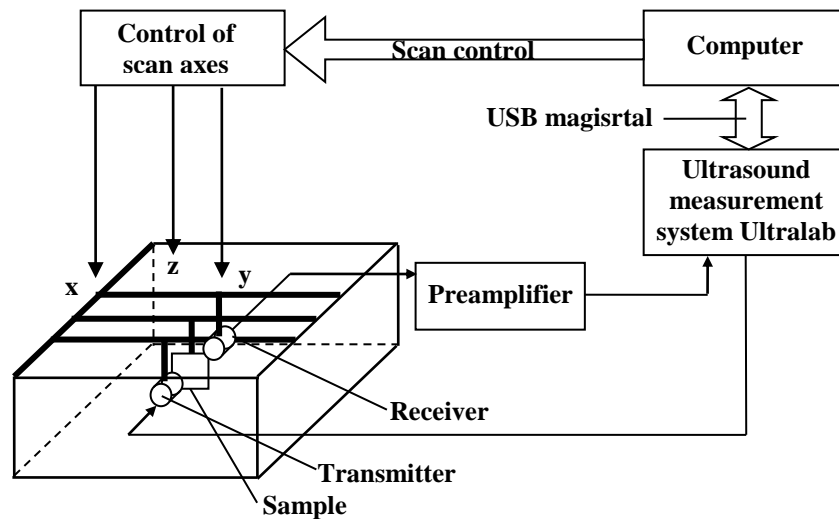


Fig.4.19. Experimental set-up of measurement system [16]

The signal was gained to 57 dB. C-scan of the inspection with 5 MHz conventional probes is shown in **Fig.4.20**.

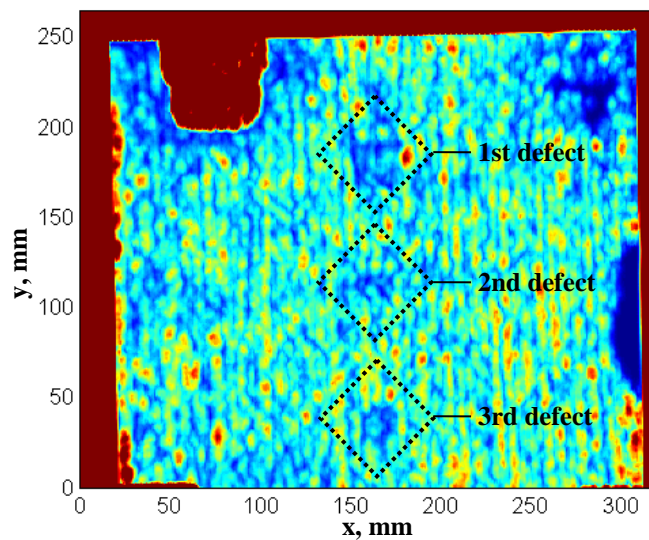


Fig.4.20. C-scan of the sample inspection with 5 MHz conventional transducer

According to C-scan of the through-transmission ultrasonic inspection, 3 delaminations are observed. The delaminations are placed in the middle of the sample along x axis and have rectangular and round shapes. There are also 2 defects on the edge of the sample which could appear because of mechanical impact when the parts of metal and composite were cut out.

The B-scan of 3 delaminations along y axis is shown in **Fig.4.21**. According to B-scan along y axis the length of 1st defect is 27 mm, 2nd defect is 17 mm and 3rd defect is 18 mm.

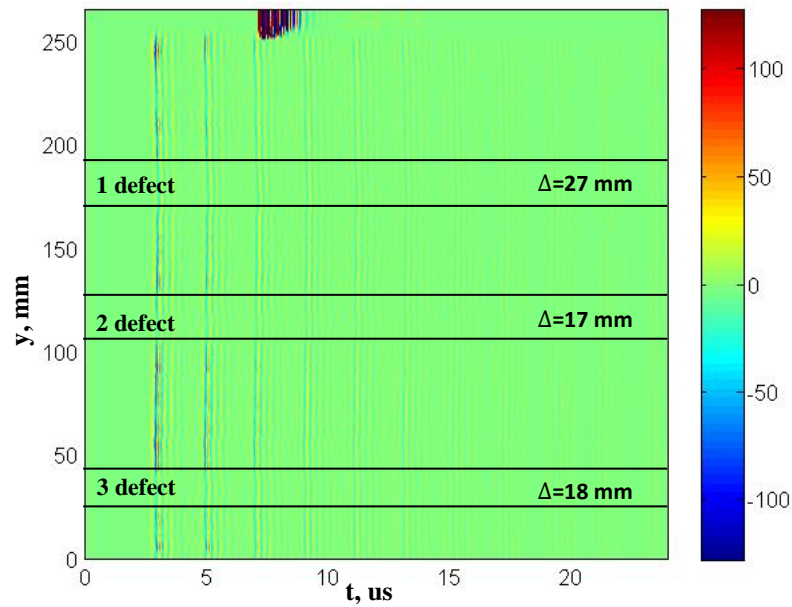


Fig.4.21. B-scan of the sample inspection with 5MHz conventional transducer along y axis

For the better resolution of delaminations only the delamination part of the sample was inspected. The signal was gained to 68dB. C-scan of the inspection with 10MHz focused probes is shown in **Fig.4.22.**

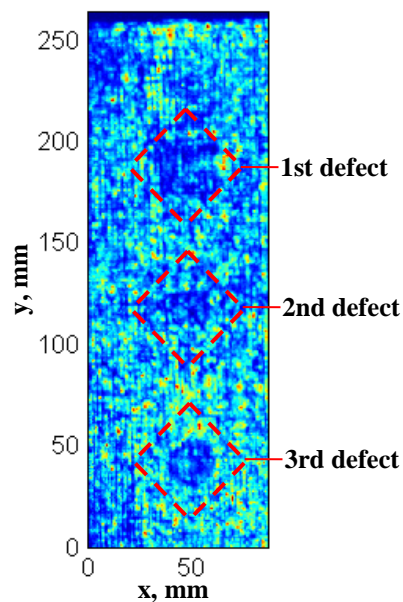


Fig.4.22. C-scan of the sample inspection with 10 MHz focused transducer

According to C-scan of the inspection, 3 delaminations are observed. First and the second delaminations have rectangular shape and the third one has round shape. Because of low amplitude difference between interface and defects it is difficult to distinguish them. The B-scan of 3 delaminations along y axis is shown in **Fig.4.23.**

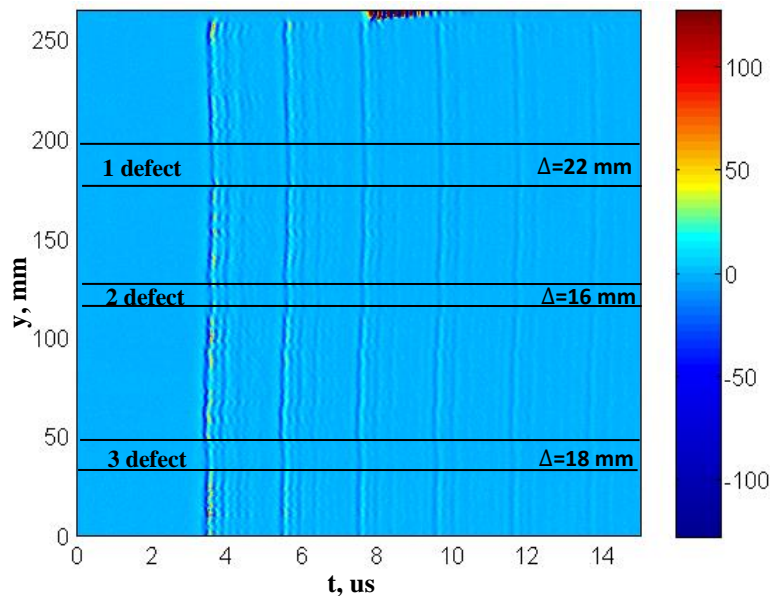


Fig.4.23. B-scan of the sample inspection with 10 MHz focused transducer along y axis

According to B-scan along y axis the length of 1st defect is 22 mm, 2nd defect is 16 mm and 3rd defect is 18 mm. The lengths of delaminations are approximate because of the reasons of signal amplification and complexity to distinguish defects.

4.6 Conclusions

As a result pulse echo ultrasonic inspections with 3,5 MHz and 5 MHz phased array transducers as well as using through transmission technique were performed. The amplitude difference between reflection from the interface and reflection from delamination is very small. The reason is in nearly equal values of reflection coefficients of defected and good interface [19], [24]. Due to it the signal was amplified to locate delaminations.

According to equation (4.5) the depths of defects were calculated. In the case of inspection using 5MHz phased array transducer the depth of 1st delamination is 6,21 mm, 2nd and 3rd delamination is 6,26 mm. The length of 1st delamination is 25,53 mm, 2nd – 15,22 mm, 3rd – 19,59 mm. In the case of inspection using 3,5 MHz phased array transducer the depth of 1st delamination is 6,24 mm, 2nd and 3rd delamination is 6,25 mm. The length of 1st delamination is 25,62 mm, 2nd – 15,24 mm, 3rd – 20,43 mm.

According to results of through-transmission ultrasonic inspection all delaminations are placed in the middle of the sample along x axis and have rectangular and round shapes. The approximate values of length of 1st delamination is 22 mm, 2nd – 16 mm, 3rd – 18 mm.

5 EVALUATION OF THE UNCERTAINTY OF THE MEASUREMENT RESULTS

The information on the measurement uncertainties of all conditions and results of measurements in ultrasonic non-destructive testing are calculated. Error is a parameter associated with a measuring instruments and characterizing the deviation of measured value from its real value. Measurement uncertainty is a parameter associated with a result of measurements and characterizing the dispersion of the values that can be attributed to a measured quantity.

There are two types of measurement uncertainties:

- Type A or direct measurements. Standard uncertainties are estimated in the measurement process using statistical analysis of multiple measurements.
- Type B or indirect measurements. Standard uncertainties are estimated using other educational sources as certificates, manuals, license, the results of previous measurements, technical documentation of the manufacturer, and others [27], [28].

5.1 Probability of detection curves computation in CIVA software

Probability of detection (POD) of delaminations in the joint of dissimilar materials is evaluated in CIVA software using POD features. Basic steps of the POD simulation in CIVA software as following:

- definition of characteristic parameter (flaw size);
- definition of variable parameters in a specific range (uncertain parameters);
- description of uncertainty distribution for variable parameters;
- using Monte-Carlo method for parameters;
- analysing resulting data and computing the POD [21].

As a characteristic value the length of delamination was selected. Position of phased array transducer on axis x, sound velocity in steel, frequency and focus depth of phased arrays are the sources of uncertainty (uncertain parameters).

Definition of characteristic and uncertain parameters as well as description of uncertainty distribution for uncertain parameters is presented in **Table 5.1**.

Four uncertain parameters affect on probability of detection of delamination length from 1 to 26 mm. In the case of inspection with 3,5 MHz phased array transducer plot of POD curve is shown in **Fig.5.1**. The POD curve is computed with confidence level of 95 %.

As a result in the case of inspection using 3,5 MHz phased array transducer POD of delamination length from 5 to 25 mm is in the range from 37-50 %.

Table 5.1. Sources of errors

Description	Parameter type	Type	Start value, mm		Stop value, mm		Step	
Delamination length, mm	Characteristic value	Linear	1		26		0,862	
Description	Parameter type	Distribution type	Mean value		Max value		Min value	
Transducer position on axis x, mm	Uncertain value	Rectangular	110		113		107	
Ultrasound velocity, m/s	Uncertain value	Normal	5 900		6 200		5 800	
Focus depth, mm	Uncertain value	Normal	6,3		7,3		5,3	
Frequency, MHz	Uncertain value	Normal	f_1	f_2	f_1	f_2	f_1	f_2
			3,5	5	3,87	5,33	3,13	4,67

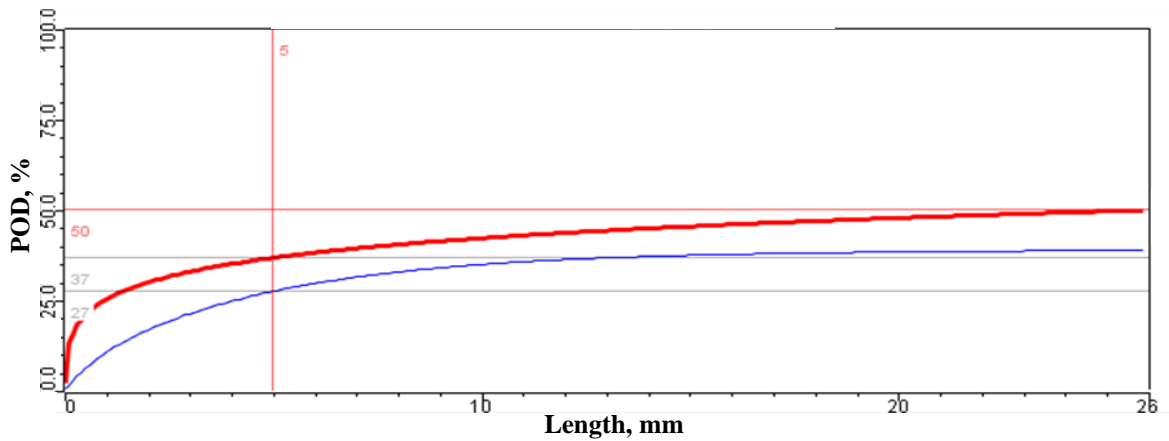


Fig.5.1. Plot of POD curve in the case of inspection with 3,5 MHz phased array

In the case of inspection with 5 MHz phased array transducer plot of POD curve is shown in **Fig.5.2.** The POD curve is computed with confidence level of 95 %.

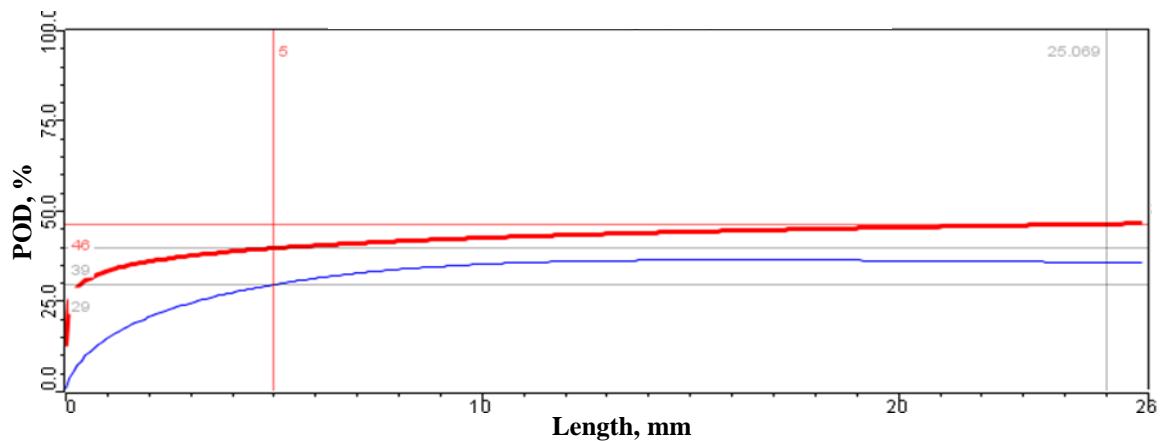


Fig.5.2. Plot of POD curve in the case of inspection with 5 MHz phased array

As a result in the case of inspection using 5 MHz phased array transducer POD of delamination length from 5 to 25 mm is in the range from 39-46 %.

5.2 Uncertainty evaluation of experimental ultrasonic testing

The uncertainty measurement of ultrasonic inspection of dissimilar material joints shows the impossibility of knowing the exact value of particular characteristics. The uncertainty evaluation for characterization of delaminations was performed to characterise the measurement results as complete and correct. A number of errors can affect the measurements and final result of ultrasound inspection [27], [29], [30]. Ultrasound testing was performed in the laboratory and consists of Omniscan measurement system, phased array transducers and specimen under inspection. Ultrasound inspection uses the sound waves to identify delaminations in the joint of dissimilar materials.

In **Table 5.2** the sources of errors which influence on the identifying of delaminations depth and lengths are presented.

Table 5.2. Sources of errors

Depth of delaminations $H_{del} = \frac{\lambda \times f \times \tau_{tofd}}{2}$			
№	Sources of errors	Uncertainty type	Model
1	Wavelength of ultrasound in steel	B	$\lambda = c_{met} / f$
2	Ultrasound velocity in steel c_{met}	B	$c_{met} = 2H_{met} / \tau_{tofd}$
3	Thickness of metal layer H_{met}	A	Statistical analysis of multiple measurements
	Resolution of calliper	B	Readings of instrument, $r = 0,01$
4	Time of flight to interface of the object	A	Statistical analysis of multiple measurements
	Resolution of display of Omniscan measurement system	B	Readings of instrument, $r = 0,01$
5	Transducer frequency f	B	Data from technical documentation
6	Time of flight to delamination of the object	A	Statistical analysis of multiple measurements
	Resolution of display of Omniscan measurement system	B	Readings of instrument, $r = 0,01$
Length of delaminations L_{del}			
№	Sources of errors	Uncertainty type	Model
1	Length of delamination from S-scan	A	Statistical analysis of multiple measurements
2	Resolution of display of Omniscan measurement system	B	Readings of instrument, $r = 0,01$
3	Pitch of phased array	B	Data from technical documentation

Error sources which affect depth and length uncertainty measurements are summarized. Errors are classified into two types: random and systematic. Random error in measurements is caused by random and unpredictable changes in experimental evaluations. Systematic error is a part of error of measurement result, which doesn't change or changes naturally in repeated measurements of the same value. The reason is in instrument faulty, wrong use or its data processing system. The uncertainty of part of error sources is calculated according to data from technical documentation of instruments and its readings. Other part of sources is calculated according to statistical analysis of multiple measurements [27], [31].

For direct measurements the arithmetic mean \bar{x} of measured results is calculated according to equation:

$$\bar{x} = \frac{1}{N} \sum_{i=1}^N x_i, \quad (5.1)$$

where N is a number of measurements, x_i is measured value.

Standard uncertainty $u(x)$ for direct measurement is calculated according to equation:

$$u(x) = \sqrt{\frac{1}{N(N-1)} \sum_{i=1}^N (x_i - \bar{x})^2} \quad (5.2)$$

Uncertainty of instrument resolution r is calculated with rectangular distribution law according to equation:

$$u(r) = \frac{r/2}{\sqrt{3}} \quad (5.3)$$

Combined uncertainty of direct measurements which is taken into account the resolution amendment is calculated according to equation:

$$u(y) = \sqrt{u(x)^2 + u(r)^2} \quad (5.4)$$

The thickness of metal layer H_{met} was measured several times with electronic calliper. In

Table 5.3 the results of measurements and combined uncertainty are presented.

Table 5.3. Uncertainty and measurement results

№	Results of multiple measurements, mm	Mean value \bar{H}_{met}, mm	Standard uncertainty $u(H_{met})$, mm	Uncertainty of calliper resolution $u(r)$, mm	Combined uncertainty $u(y)$, mm
1	6,31	6,30	0,0126	0,0029	0,0129
2	6,37				
3	6,28				
4	6,27				
5	6,30				
6	6,30				
7	6,28				

As a result seven independent measurements of metal height were obtained with electronic calliper. Resolution of calliper is affects combined uncertainty as well. Mean value of metal height and uncertainties were calculated according to equations (5.1-5.4).

Time of flight to interface of the object and back to transducer τ_{tofi} was measured with Omniscan measurement system several times as well. In **Table 5.4** the results of measurements and combined uncertainty are presented.

Table 5.4. Uncertainty and measurement results

№	Results of multiple measurements, us	Mean value $\bar{\tau}_{tofi}$, us	Standard uncertainty $u(\tau_{tofi})$, us	Uncertainty of Omniscan display resolution $u(r)$, us	Combined uncertainty $u(y)$, us
1	2,06	2,0571	0,0036	0,0029	0,0046
2	2,06				
3	2,06				
4	2,04				
5	2,07				
6	2,05				
7	2,06				

Seven independent measurements of time of flight of ultrasound to interface and back to transducer were performed with Omniscan measurement system according to equation (4.2). On A-scan the initial starting point was taken at zero crossing. Resolution of Omniscan display affects combined uncertainty as well. Mean value of time of flight and uncertainties were calculated according to equations (5.1-5.4).

In the case of inspection with 3,5 MHz phased array transducer, time of flight to delaminations of the object and back to transducer τ_{tofd} was measured with Omniscan measurement system several times as well. In **Table 5.5** the results of measurements and combined uncertainty of all delaminations of the object are presented.

Table 5.5. Uncertainty and measurement results in the case of inspection with 3,5 MHz phased array transducer

№	Results of multiple measurements, us			Standard uncertainty $u(\tau_{tofd})$, us	Uncertainty of Omniscan display resolution $u(r)$, us	Combined uncertainty $u(y)$, us
	1st defect	2nd defect	3rd defect			
1	2,05	2,03	2,04	0,0056	0,0029	0,0063
2	2,02	2,03	2,04			
3	2,04	2,05	2,04			
4	2,08	2,07	2,03			
5	2,05	2,03	2,04			
6	2,01	2,04	2,05			
7	2,03	2,04	2,05			
	Mean value $\bar{\tau}_{tofd}$, us					
	2,0386	2,0414	2,0414			

In the case of inspection with 5 MHz phased array transducer, time of flight to delaminations of the object and back to transducer τ_{tofd} was measured with Omniscan measurement system several times as well. In **Table 5.6** the results of measurements and combined uncertainty of all delaminations of the object are presented.

Table 5.6. Uncertainty and measurement results in the case of inspection with 5 MHz phased array transducer

№	Results of multiple measurements, us			Standard uncertainty $u(\tau_{tofd})$, us	Uncertainty of Omniscan display resolution $u(r)$, us	Combined uncertainty $u(y)$, us
	1st defect	2nd defect	3rd defect			
1	2,04	2,04	2,04	0,0060	0,0029	0,0067
2	2,02	2,02	2,04			
3	2,05	2,05	2,05			
4	2,01	2,05	2,04			
5	2,05	2,04	2,04			
6	2,04	2,05	2,05			
7	2,04	2,05	2,04			
	Mean value $\bar{\tau}_{tofd}$, us					
	2,0357	2,0428	2,0429			

Seven independent measurements of time of flight to 3 delaminations of the object were obtained with Omniscan measurement system according to equation (4.2). On A-scan the initial starting point was taken at zero crossing. Resolution of Omniscan display affects combined uncertainty as well. Mean value for each delamination of time of flight and uncertainties were calculated according to equations (5.1-5.4).

If the range of values has equal probability, then the rectangular distribution law is used for the B type uncertainty estimation [27]. Standard uncertainty $u(x)$ is calculated according to equation:

$$u(x) = \frac{\Delta}{\sqrt{3}}, \quad (5.5)$$

where Δ is an error of value x .

Influence coefficient of x value $W(x)$ is calculated according to equation:

$$W(x) = \frac{\partial f}{\partial x}, \quad (5.6)$$

where f is a function or model of uncertainty measurement.

Combined uncertainty of B type measurements (indirect measurements) of x values is calculated according to equation:

$$u(y) = \sqrt{\sum_{i=1}^n u(x_i)^2 \times W(x_i)^2} \quad (5.7)$$

In **Table 5.7** the results of uncertainties of B type measurement of ultrasound velocity c_{met} are presented.

Table 5.7. Measurement results of ultrasound velocity uncertainties

Measurement model of c_{met}	Sources of errors	Standard uncertainty $u(x)$	Influence coefficient $W(x)$	Combined uncertainty $u(y)$, mm/us
$c_{met} = 2H_{met} / \tau_{tofi}$	Thickness H_{met} , mm	0,0129	0,9722	0,0186
	Time of flight τ_{tofi} , us	0,0046	2,9782	

Combined uncertainty of measurement model of c_{met} is calculated according B type procedure. Influence coefficients of error sources of metal thickness and time of flight to interface and back to transducer as well as combined uncertainty are calculated according to equations (5.6-5.7). Standard uncertainties of these values are calculated and taken from Table 5.3 and Table 5.4.

In **Table 5.8** the results of uncertainties of B type measurement of wavelength λ in steel are presented:

Table 5.8. Measurement results of wavelength uncertainties

Measurement model of λ	Sources of errors	Error Δ	Standard uncertainty $u(x)$	Influence coefficient $W(x)$		Combined uncertainty $u(y)$, mm	
				f_1	f_2	f_1	f_2
$\lambda = c_{met} / f$	Sound velocity in steel c_{met} , mm/us	-	0,0186	f_1	f_2	0,0289	0,0487
				0,1919	0,2618		
	Frequency f_1 of 5.21MHz	0,22	0,1270	0,2256			
	Frequency f_2 of 3.82MHz	0,2	0,1154	0,4197			

Combined uncertainty of measurement model of λ is calculated according B type procedure. Rectangular distribution $\frac{1}{\sqrt{3}}$ is selected for estimating standard uncertainty of frequencies, $f_1 = 5,21$ MHz and $f_2 = 3,82$ MHz. Values of frequency errors are taken from technical documentations of phased array transducers. Influence coefficients of error sources of sound velocity and frequencies as well as standard and combined uncertainties are calculated according to equations (5.5-5.7). Standard uncertainties of sound velocity in metal is calculated and taken from Table 5.7. Ultrasonic wavelength in metal of 3,82 MHz frequency is 1,6034 mm, 5,21 MHz frequency is 1,1756 mm.

The expanded uncertainty of the model is calculated according to equation [27], [31]:

$$u_{\text{exp}} = k \times u(y), \quad (5.8)$$

where k is expansion coefficient, $u(y)$ is combined uncertainty of the model.

Measurement model consists of several input variables and due to it the expansion coefficient k is selected from the Student table according to confidence probability and effective number of degrees of freedom [27], [31]. The effective number of degrees of freedom ν_{eff} is calculated according to equation:

$$\nu_{\text{eff}} = \frac{u^4(y)}{\sum_{i=1}^n \frac{u_i^4(y)}{\nu_i}}, \quad (5.9)$$

where ν_i is a degree of freedom.

The degree of freedom for direct uncertainty measurements is calculated according to equation:

$$\nu_i = N - 1, \quad (5.10)$$

where N is a number of measurements.

The degree of freedom for B type (indirect) uncertainty measurements is calculated according to equation:

$$\nu_i = \frac{1}{2(1 - R_i)^2}, \quad (5.11)$$

where R_i is reliability of the uncertainty, $R_i = 1$ at 100% reliability.

In the case of inspection with 3,5 MHz phased array transducer the results of standard and expanded uncertainties of delamination depths are presented in **Table5.9**.

Combined uncertainties of measurement model of H_{del} are calculated according B type procedure for each delamination of the object. Values of frequency errors are taken from technical documentations of phased array transducers. Influence coefficients of error sources of wavelength, frequency and time of flight to delamination and back to transducer as well as combined uncertainties are calculated according to equations (5.5-5.7). Expansion coefficient k is selected from Student table according to results of effective number of degrees of freedom ν_{eff} and chosen probability of 95,45 % [27], [31]. As a result in the case of inspection with 3,5 MHz phased array transducer the expanded uncertainty u_{exp} of 1st delamination depth is $6,24 \pm 0,536$ (mm), of 2nd delamination depth is $6,25 \pm 0,536$ (mm), and of 3rd delamination depth is $6,25 \pm 0,536$ (mm).

Table 5.9. Measurement results of delamination depths uncertainties

Model	$H_{del} = \frac{\lambda \times f \times \tau_{tofd}}{2}$						
Sources of errors	Wavelength of ultrasound in steel λ , mm			Frequency f of 3,82MHz			Time of flight to delamination and back to transducer τ_{tofd} , us
	1st defect	2nd defect	3rd defect	1st defect	2nd defect	3rd defect	
Standard uncertainty $u(x)$	0,0487			0,1154			0,0063
Influence coefficient $W(x)$	3,8746	3,9017	3,9019	1,6263	1,6377	1,6378	3,0625
Combined uncertainty $u(y)$, mm	0,2680						
Effective number of degrees of freedom ν_{eff}	∞						
Probability p, %	95,45						
Expansion coefficient k	2						
Expanded uncertainty u_{exp}, mm	0,5360						

Uncertainty evaluation of delamination depths was obtained in GUM Workbench software used to analyze the uncertainty of measurements. Mathematical and statistical analyzes of measurements follows ISO Guide to the Expression of Uncertainty in Measurements and EA 4/02 requirement document of the European Cooperation of Accreditation [29].

The data of measurement model of delamination depth was entered in the software and the results of standard uncertainties, combined uncertainties and influence coefficients coincide with results in Tables 5.3-5.9 calculated manually. In addition Monte Carlo simulation was performed in GUM Workbench software for 3 delaminations. In the case of inspection with 3,5 MHz phased array transducer the results of Monte Carlo simulation for delaminations depth are presented in **Table 5.10**.

As a result interval of expanded uncertainty was calculated in GUM Workbench software and also simulated in the same software according to Monte Carlo method and the results obtained are slightly different. Plots of Monte Carlo simulation for all delamination depth are shown in **Fig.5.3-5.5**.

Table 5.10. Monte Carlo simulation results

Delamination number	Mean value, mm	Standard uncertainty, mm	Probability p, %	Expanded uncertainty interval, mm	
				Monte Carlo	GUM Workbench
1st	6,24	0,27	95,45	+0,54, -0,52	+0,54, -0,54
2nd	6,25				
3rd	6,25				

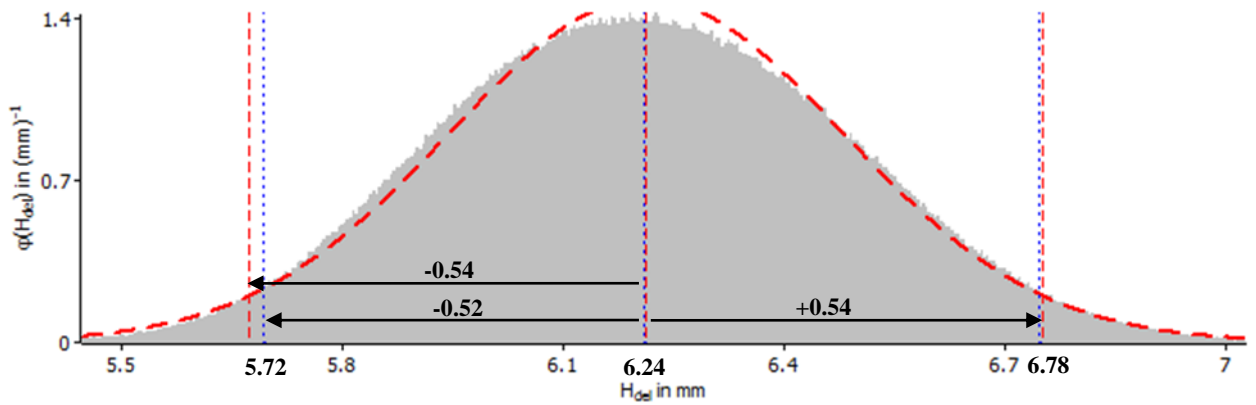


Fig.5.3. Monte Carlo simulation plot for 1st delamination depth

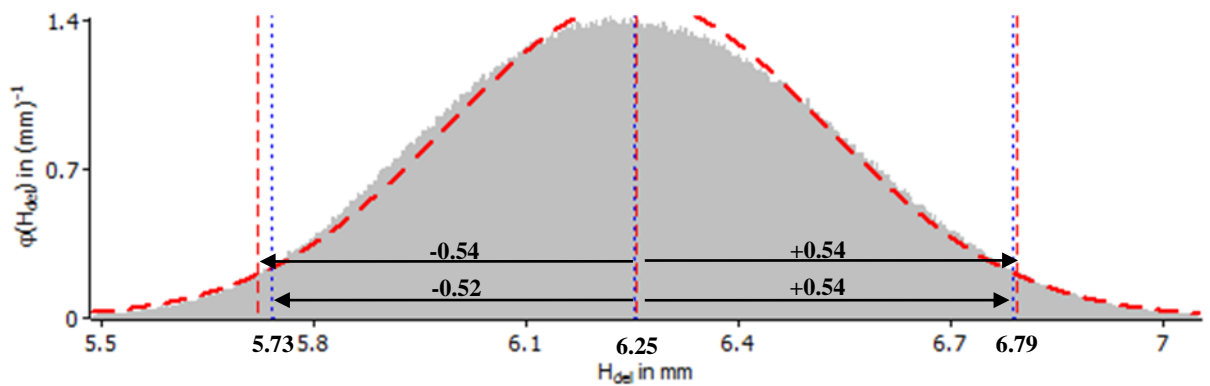


Fig.5.4. Monte Carlo simulation plot for 2nd delamination depth

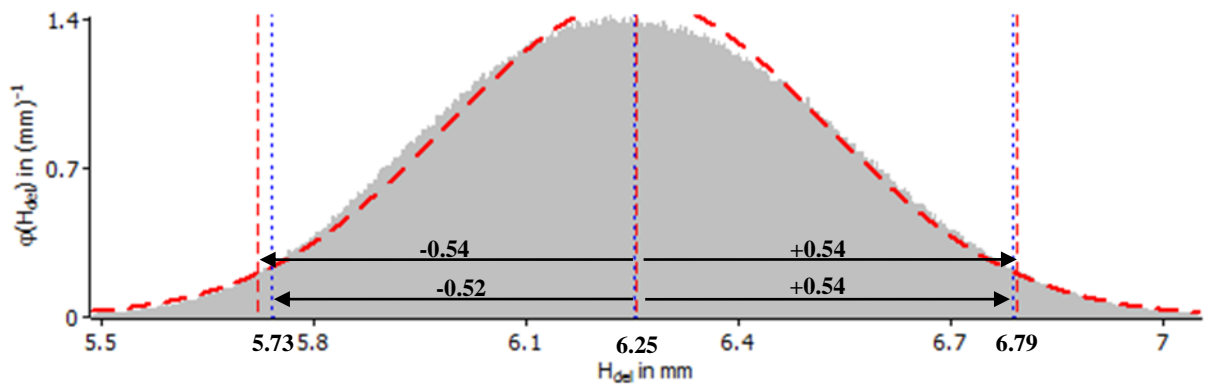


Fig.5.5. Monte Carlo simulation plot for 3rd delamination depth

In the case of inspection with 5 MHz phased array transducer the results of standard and expanded uncertainties of delamination depths are presented in **Table 5.11**.

Table 5.11. Measurement results of delamination depths uncertainties

Model	$H_{del} = \frac{\lambda \times f \times \tau_{tof}}{2}$						
Sources of errors	Wavelength of ultrasound in steel λ , mm			Frequency f of 5,21MHz			Time of flight to delamination and back to transducer τ_{tof} , us
	1st defect	2nd defect	3rd defect	1st defect	2nd defect	3rd defect	
Standard uncertainty $u(x)$	0,0289			0,1270			0,0067
Influence coefficient $W(x)$	5,2845	5,3215	5,3218	1,1924	1,2008	1,2008	3,0624
Combined uncertainty $u(y)$, mm	0,2170						
Effective number of degrees of freedom ν_{eff}	∞						
Probability p , %	95,45						
Expansion coefficient k	2						
Expanded uncertainty u_{exp} , mm	0,4340						

Combined uncertainties of measurement model of H_{del} are calculated according B type procedure for each delamination of the object. Values of frequency errors are taken from technical documentations of phased array transducers. Influence coefficients of error sources of wavelength, frequency and time of flight to delamination and back to transducer as well as combined uncertainties are calculated according to equations (5.5-5.7). Expansion coefficient k is selected from Student table according to results of effective number of degrees of freedom ν_{eff} and chosen probability of 95,45 % [27], [31]. In the case of inspection with 5 MHz phased array transducer the expanded uncertainty u_{exp} of 1st delamination depth is $6,23 \pm 0,434$ (mm), of 2nd delamination depth is $6,25 \pm 0,434$ (mm), and of 3rd delamination depth is $6,25 \pm 0,434$ (mm).

The data of measurement model of delamination depth was entered in GUM Workbench software and the results of standard uncertainties, combined uncertainties and influence coefficients coincide with results in Tables 5.3-5.8 and Table 5.13 calculated manually. In addition Monte Carlo simulation was performed in GUM Workbench software for 3 delaminations. In the case of inspection with 5 MHz phased array transducer the results of Monte Carlo simulation for delaminations depth are presented in **Table 5.12**.

Table 5.12. Monte Carlo simulation results

Delamination number	Mean value, mm	Standard uncertainty, mm	Probability p, %	Expanded uncertainty interval, mm	
				Monte Carlo	GUM Workbench
1st	6,23	0,22	95,45	+0,43, -0,42	+0,44, -0,44
2nd	6,25				
3rd	6,25				

As a result interval of expanded uncertainty was calculated in GUM Workbench software and also simulated in the same software according to Monte Carlo method and the results obtained are slightly different. Plots of Monte Carlo simulation for delaminations depth are shown in **Fig.5.6** and **Fig.5.7** respectively.

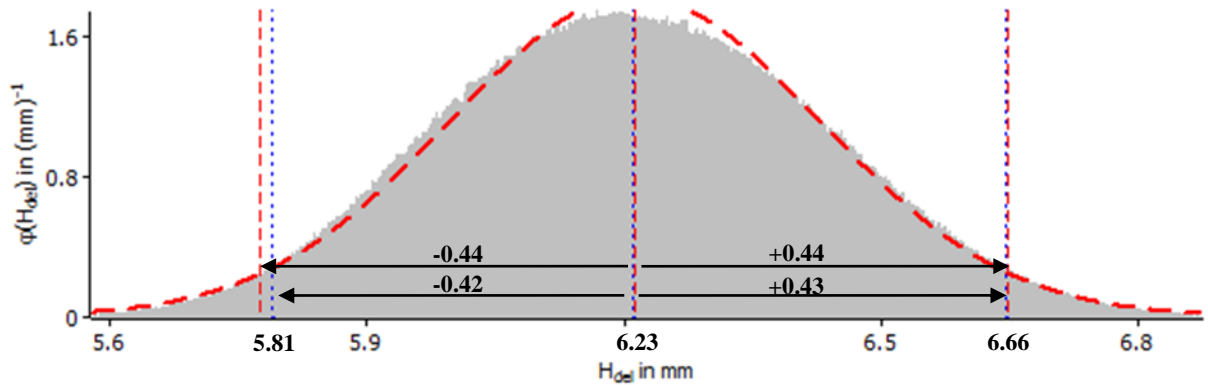


Fig.5.6. Monte Carlo simulation plot for 1st delamination depth

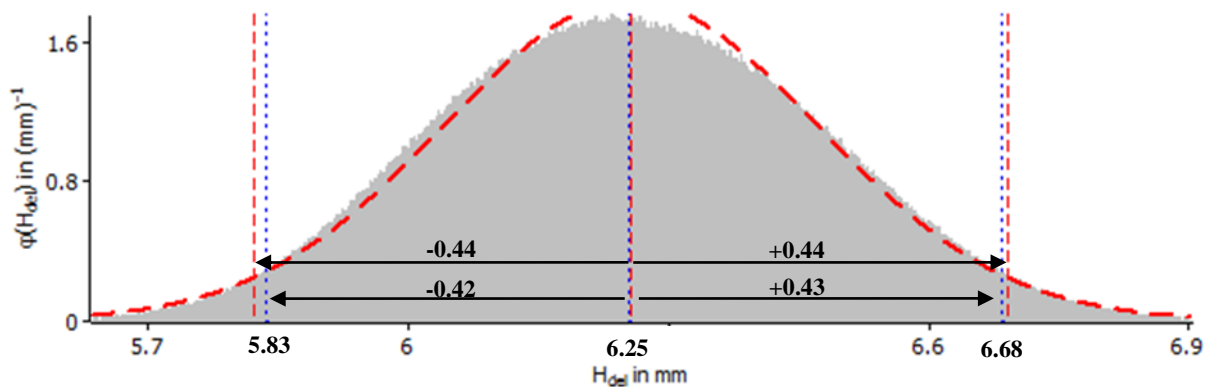


Fig.5.7. Monte Carlo simulation plot for 2nd and 3rd delaminations depth

In the case of inspection with 3,5 MHz phased array transducer the lengths of delaminations L were measured several times from S-scan of Omniscan measurement system. In **Table 5.13** the results of measurements and combined uncertainty are presented:

Table 5.13. Uncertainty and measurement results

№	Results of multiple measurements, mm			Standard uncertainty $u(L_{del})$, mm	Uncertainty of Omniscan display resolution $u(r)$, mm	Combined uncertainty $u(y)$
	1st defect	2nd defect	3rd defect			
1	25,86	15,18	20,59	0,1078	0,0029	0,1078
2	25,57	15,12	20,34			
3	25,35	15,28	20,01			
4	25,07	15,76	20,31			
5	25,82	15,03	20,24			
6	26,01	15,19	20,73			
7	25,63	15,09	20,81			
	Mean value \bar{L}_{del}					
	25,62	15,24	20,43			

Seven independent measurements of lengths of delaminations were obtained with Omniscan measurement system. Resolution of Omniscan display affects on combined uncertainty as well. Mean value of length for each delamination and uncertainties were calculated according to equations (5.1-5.4).

In **Table 5.14** the results of standard and expanded uncertainties of delamination lengths are presented.

Table 5.14. Measurement results of delamination lengths uncertainties

Model	$L_{del} = L_{del} + y$, where y is amendment of pitch of transducers		
Sources of errors	Length of delamination from S-scan L_{del}	Pitch of phased array p	
		Error Δ	0,01
Standard uncertainty $u(x)$	0,1078	0,006	
Combined uncertainty $u(y)$	0,1080		
Number of degrees of freedom ν	6		
Probability p, %	95,45		
Expansion coefficient k	2,52		
Expanded uncertainty u_{exp}	0,2722		

Combined uncertainties of delamination lengths are calculated according A type procedure. Two amendments (display resolution and phased array pitch) were taken into account due to their affect on result [29], [30]. Standard uncertainty of phased arrays pitch was calculated according to equation (5.5). Combined uncertainties of delamination lengths and number of degrees of freedom for A type procedure were calculated according to equation (5.4) and equation (5.10) respectively. Confidence probability of 95,45 % was chosen and expansion coefficient k was selected from Student table according to result of number of degrees of freedom. As a result the expanded uncertainty of 1st delamination length is $25,62 \pm 0,2722$ (mm),

of 2nd delamination length is $15,24 \pm 0,2722$ (mm), and of 3rd delamination length is $20,43 \pm 0,2722$ (mm).

The data of measurement model of delamination length was entered in GUM Workbench software. Results of standard uncertainties are coincides with results in Tables 5.17 and Table 5.18 calculated manually. The expanded uncertainty differs from the results calculated manually due to expansion coefficient $k=2$ and probability of 95 % selected in GUM Workbench software. In addition Monte Carlo simulation was performed in GUM Workbench software for 3 delaminations. The results of Monte Carlo simulation for all delaminations length are presented in **Table 5.15**.

As a result interval of expanded uncertainty was calculated in GUM Workbench software and also simulated in the same software according to Monte Carlo method. The results of Monte Carlo simulation coincides with results calculated manually.

Table 5.15. Monte Carlo simulation results

Delamination number	Mean value, mm	Standard uncertainty, mm	Expanded uncertainty interval, mm	
			Monte Carlo, probability 95,45 %	GUM Workbench, probability 95%
1st	25,62	0,11	+0,27, -0,27	+0,22, -0,22
2nd	15,24			
3rd	20,43			

Plots of Monte Carlo simulation for delaminations length are shown in **Fig.5.8-5.10**.

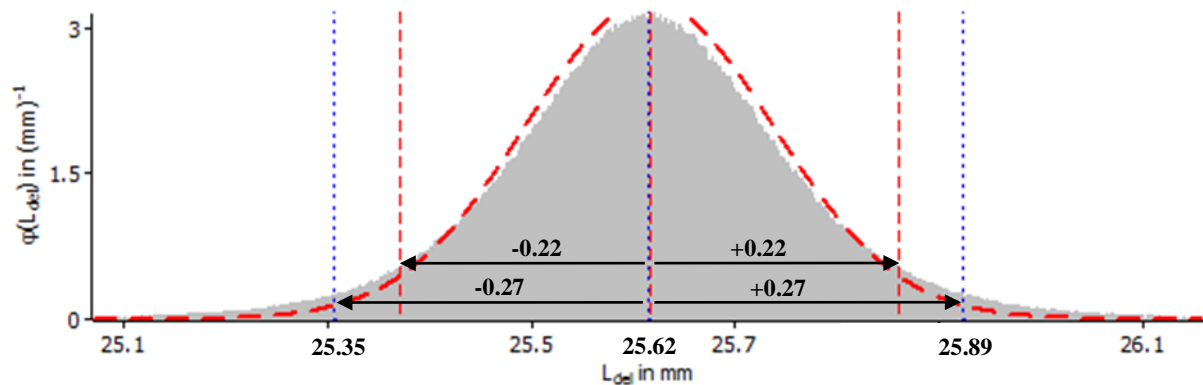


Fig.5.8. Monte Carlo simulation plot for 1st delamination length

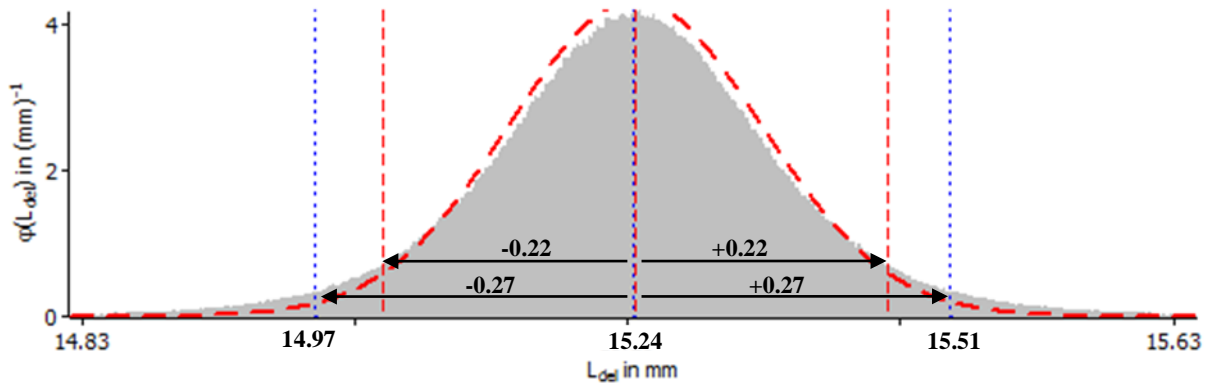


Fig.5.9. Monte Carlo simulation plot for 2nd delamination length

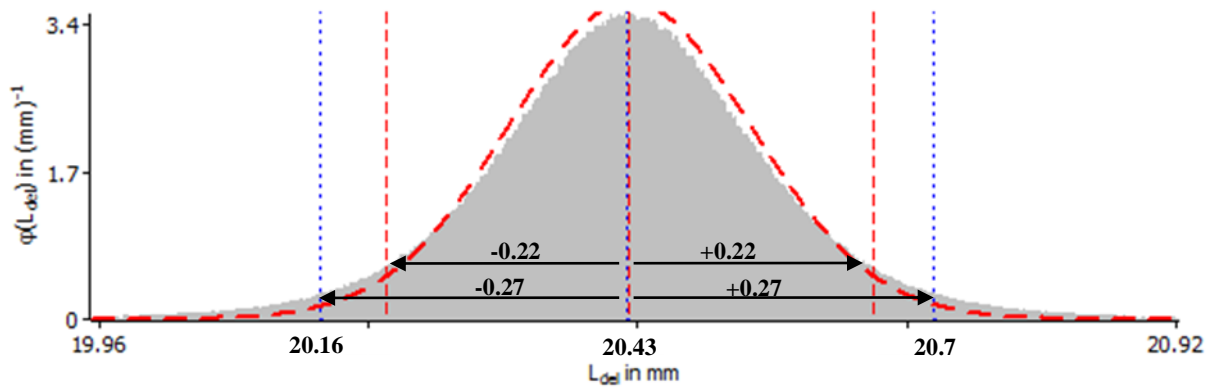


Fig.5.10. Monte Carlo simulation plot for 3rd delamination length

In the case of inspection with 5 MHz phased array transducer the lengths of delaminations L were measured several times from S-scan of Omniscan measurement system. In **Table 5.16** the results of measurements and combined uncertainty are presented:

Table 5.16. Uncertainty and measurement results

№	Results of multiple measurements, mm			Standard uncertainty $u(L_{del}), \text{ mm}$	Uncertainty of Omniscan display resolution $u(r), \text{ mm}$	Combined uncertainty $u(y)$
	1st defect	2nd defect	3rd defect			
1	25,51	15,14	19,06	0,0860	0,0029	0,0860
2	25,62	15,07	19,37			
3	25,37	15,16	20,06			
4	25,47	15,35	19,49			
5	25,58	15,51	20,07			
6	25,67	15,23	19,16			
7	25,49	15,11	19,93			
	Mean value \bar{L}_{del}					
	25,53	15,22	19,59			

Seven independent measurements of lengths of delaminations were obtained with Omniscan measurement system. Resolution of Omniscan display affects on combined uncertainty as well. Mean value of length for each delamination and uncertainties were calculated according to equations (5.1-5.4).

In **Table 5.17** the results of standard and expanded uncertainties of delamination lengths are presented.

Table 5.17. Measurement results of delamination lengths uncertainties

Model	$L_{del} = L_{del} + y$, where y is amendment of pitch of transducers	
Sources of errors	Length of delamination from S-scan L_{del}	Pitch of phased array p
		Error Δ
Standard uncertainty $u(x)$	0,0860	0,006
Combined uncertainty $u(y)$	0,0862	
Number of degrees of freedom ν	6	
Probability p , %	95,45	
Expansion coefficient k	2,52	
Expanded uncertainty u_{exp}	0,2172	

Combined uncertainties of delamination lengths are calculated according A type procedure. Two amendments (display resolution and phased array pitch) were taken into account due to their affect on result [29], [30]. Standard uncertainty of phased arrays pitch was calculated according to equation (5.5). Combined uncertainties of delamination lengths and number of degrees of freedom for A type procedure were calculated according to equation (5.4) and equation (5.10) respectively. Confidence probability of 95,45 % was chosen and expansion coefficient k was selected from Student table according to result of number of degrees of freedom. As a result the expanded uncertainty of 1st delamination length is $25,53 \pm 0,2172$ (mm), of 2nd delamination length is $15,22 \pm 0,2172$ (mm), and of 3rd delamination length is $19,59 \pm 0,2172$ (mm).

The data of measurement model of delamination length was entered in GUM Workbench software. Results of standard uncertainties are coincides with results in Tables 5.20 and Table 5.21 calculated manually. The expanded uncertainty differs from the results calculated manually due to expansion coefficient $k=2$ and probability of 95 % selected in GUM Workbench software. In addition Monte Carlo simulation was performed in GUM Workbench software for 3 delaminations. The results of Monte Carlo simulation for all delaminations length are presented in **Table 5.18**.

Table 5.18. Monte Carlo simulation results

Delamination number	Mean value, mm	Standard uncertainty, mm	Expanded uncertainty interval, mm	
			Monte Carlo, probability 95,45 %	GUM Workbench, probability 95 %
1st	25,53	0,09	+0,22, -0,22	+0,17, -0,17
2nd	15,22			
3rd	19,59			

As a result interval of expanded uncertainty was calculated in GUM Workbench software and also simulated in the same software according to Monte Carlo method. The results of Monte Carlo simulation coincides with results calculated manually. Plots of Monte Carlo simulation for delaminations length are shown in **Fig.5.11-5.13**.

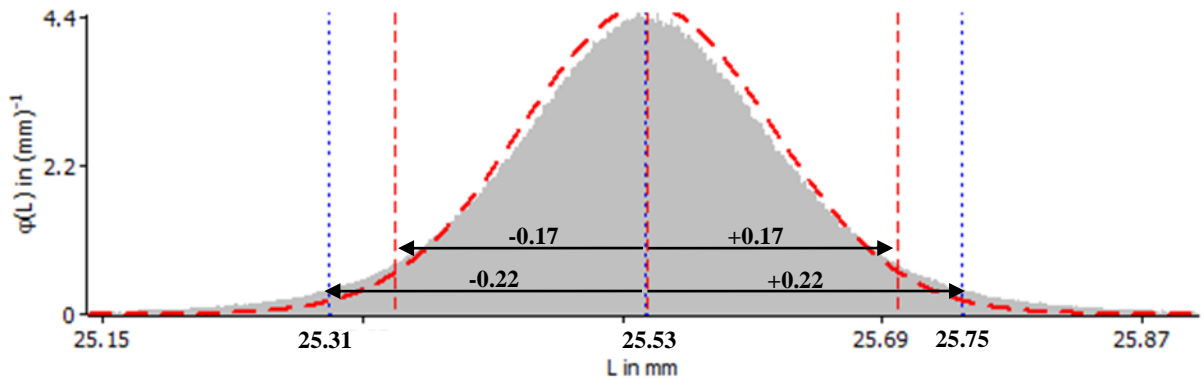


Fig.5.11. Monte Carlo simulation plot for 1st delamination length

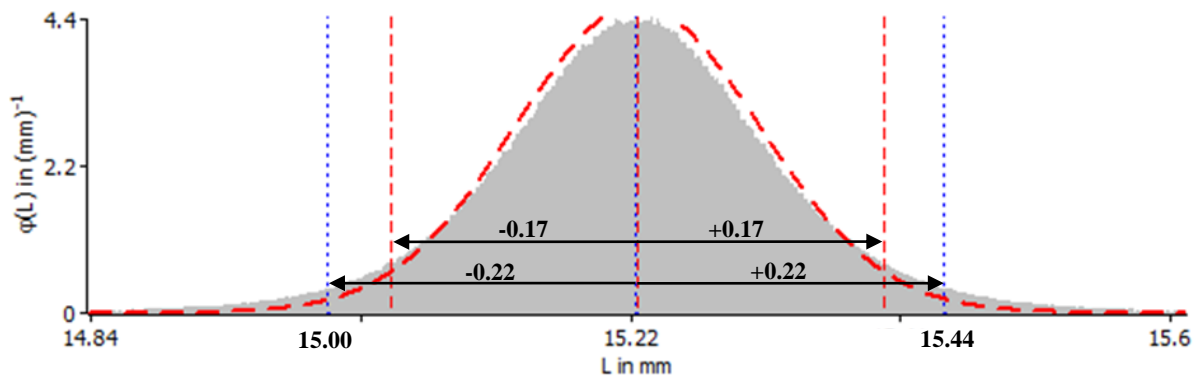


Fig.5.12. Monte Carlo simulation plot for 2nd delamination length

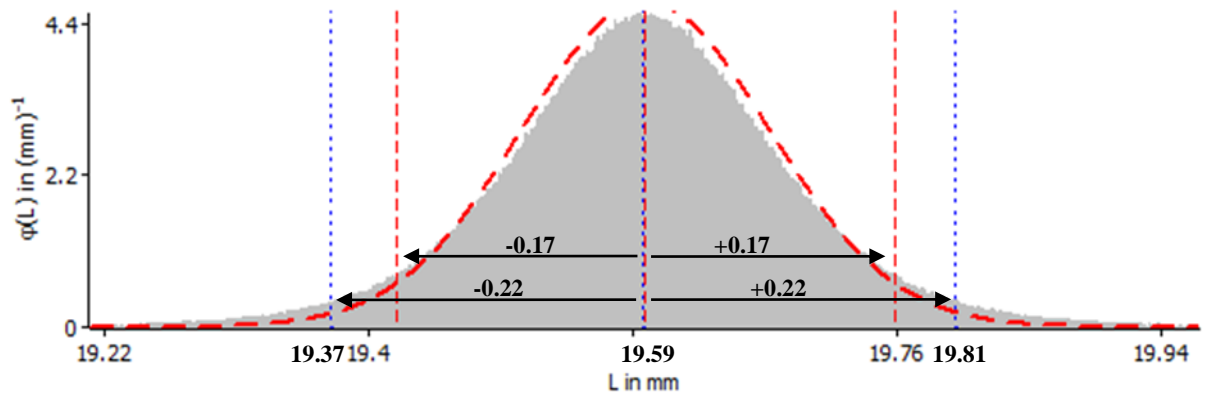


Fig.5.13. Monte Carlo simulation plot for 3rd delamination length

As a result the uncertainty of delamination depths as well as the uncertainty of delamination lengths for each delamination is calculated manually and using GUM Workbench software.

CONCLUSIONS

In this thesis the joint of steel and GFRP was inspected using ultrasonic non-destructive testing. Pulse echo ultrasonic technique has been selected as the most suitable by analyzing different ultrasonic methods and characteristics of the sample [4].

CIVA computer modelling of joint of steel and GFRP was performed using conventional and phased array transducers of different frequencies. Steel is almost 3 times less attenuating material than GFRP according to results of investigation of ultrasonic fields and influence of attenuation in dissimilar materials. Therefore the ultrasonic inspection from metal side has been performed. In addition to that increasing the frequency of transducer the attenuation value increases as well [16], [17]. As a result of this and taken into account sample thickness as well as ultrasonic wavelength 3,5 MHz and 5 MHz frequencies have been selected as the most suitable for the inspection of joint of dissimilar materials.

According to the type and dimension of defects phased array transducers were used for the inspection due to their ability of steering of multiple elements, focusing and covering large area of the sample without mechanical scanning [16], [24].

It was determined, that amplitude difference between reflection from the delaminations and reflection from the interface without defect is in the range of 0,1-1,7 dB what proves the complexity of defect location in experimental part [4]-[6].

In experimental part the Omniscan measurement system and phased arrays were used for the inspection of the sample. As a result the delaminations were located and depths and lengths of delaminations have been measured. In addition to that the uncertainties of all measurements were evaluated.

In the case of inspection with 3,5 MHz phased array transducer the depth of 1st delamination is $6,24 \pm 0,54$ (mm), of 2nd is $6,25 \pm 0,54$ (mm), and of 3rd is $6,25 \pm 0,54$ (mm). The length of 1st delamination is $25,62 \pm 0,27$ (mm), of 2nd is $15,24 \pm 0,27$ (mm), and of 3rd is $20,43 \pm 0,27$ (mm).

In the case of inspection with 5 MHz phased array transducer the depth of 1st delamination is $6,23 \pm 0,43$ (mm), of 2nd delamination is $6,25 \pm 0,43$ (mm), and of 3rd delamination is $6,25 \pm 0,43$ (mm). The length of 1st delamination is $25,53 \pm 0,22$ (mm), of 2nd is $15,22 \pm 0,22$ (mm), and of 3rd is $19,59 \pm 0,22$ (mm).

REFERENCES

1. Ravi Prakash, "Non-Destructive Testing Techniques". New Age Science Limited, UK., 2009. – 140 p.
2. C.C.H. Guyott, "The non-destructive testing of adhesively bonded structures". Department of Mechanical Engineering, Imperial College of Science and Technology, London SW7, November 1986. – 222 p.
3. Dr. L. John Hart-Smith, "Adhesively Bonded Joints in Aircraft Structures". Handbook of Adhesion Technology, Springer Berlin Heidelberg, 2011, p. 1101-1147
4. C.V. Subramanian, "Practical Ultrasonics". Alpha Science International Ltd. Oxford, U.K., 2006. – 150 p.
5. Ultrasonic Thickness Gaging. Olympus Corporation. [Viewed February 19, 2015]. - <https://www.olympus-ims.com/>
6. Samsir Tanary, "Characterization of adhesively bonded joints using Acousto-ultrasonics". Department of Mechanical Engineering, University of Ottawa, Canada, April 1990. – 216 p.
7. В.В. Ключев, Ф.Р. Соснин, А.В. Ковалев и др., "Неразрушающий контроль и диагностика". 2-е изд., испр. и доп. – М.: Машиностроение, 2003. – 653 с.
8. Ajay Kapadia, "Non Destructive testing of composite materials". National Composites Network; TWI Ltd. Chang J, Zheng C, "The ultrasonic wave propagation in composite material and its characteristic evaluation". Composite Structures; 75, No. 1-4, 2006. p. 451-456
9. Michael Berke, "Nondestructive Material Testing with Ultrasonics", p. 4-16. M. Berke, "Thickness measurement with ultrasonics" Krautkrämer Training System, Part 5 2nd edition, 1992
10. NDT course material, NDT Resource Center. [Viewed December 2, 2013]. - <http://www.ndt-ed.org/>
11. Claudia Farias, Eduardo Filho, Ygor Santos, Matheus Arauji, Igor Ribeiro, "Spectral Analysis of the propagation of Lamb Waves on Fiber-Metal Laminated Plates to detect and evaluate different defects". 18th World Conference on Nondestructive Testing, 16-20 April 2012, Durban, South Africa. p. 1-8
12. Zhongqing Su, Lin Ye, Ye Lu, "Guided Lamb waves for identification of damage in composite structure: A review". Journal of Sound and Vibration 295, Sydney, Australia, 2006. p. 753-780

13. Seth S Kessler, S Mark Spearing and Constantinos Soutis, "Damage detection in composite materials using Lamb wave methods". Institute of Physics Publishing, Smart Material and Structures, 5 April 2002. – 278 p.
14. Ingolf Hertlin, Detlev Schultze, "Acoustic Resonance Testing: the upcoming volume-oriented NDT method". 111 Pan-American Conference for Nondestructive Testing, Rio de Janeiro, 2003. – 7 p.
15. John H. Gieske and Mark A. Rumsey, "Nondestructive Evaluation (NDE) of Composite-to-Metal Bond Interface of a Wind Turbine Blade Using An Acousto-Ultrasonic Technique". Sandia National Laboratories, Albuquerque, New Mexico 87185, 1996. – 14p.
16. E. Jasiūnienė, E. Žukauskas, V. Samaitis. Ultragarsinių matavimų laboratoriniai darbai. Mokomoji knyga. Kaunas: Technologija, 2013. – 91p.
17. S.W. Rienstra, A. Hirschberg, "An Introduction to Acoustics". Eindhoven University of Technology, 26 January 2015. – 296 p.
18. Agilent Impedance Measurement Handbook, A guide to measurement technology and techniques, 4th Edition. Agilent Technologies Inc. 2009-2013 Published in USA, September 10, 2013, 5950-3000. – 140 p.
19. Acoustic Velocity, Impedance, Reflection, Transmission, Attenuation, and Acoustic Etalons. [Viewed November 8, 2014]. - <http://www.iowadoppler.com/documents/acoustic-experiments.pdf>
20. L. Satyanarayan, C. Sridhar, C.V. Krishnamurthy, Krishnan Balasubramaniam, "Simulation of ultrasonic phased array technique for imaging and sizing of defects using longitudinal waves". International Journal of Pressure Vessels and Piping 84 (2007). p. 716–729
21. CIVA 2015 User Manual (v11.1). CIVA EXTENDE, 2015. – 1144p.
22. Robert M. Jones, "Mechanics of Composite Materials". Second edition, Taylor & Francis Ltd. Virginia, USA, 1999. - 501 p.
23. Кербер М.Л., Виноградов В.М., Головкин Г.С. и др., „Полимерные композиционные материалы: структура, свойства, технологий“: учеб. Пособие. – 3-е испр. изд. – СПб.: ЦОП „Профессия“, 2011. -560с., ил.
24. Elena Jasiūnienė, "Ultragarsinė medžiagotyra". Mokomoji knyga, Kauno Technologijos Universitetas, UAB Vitae Litera, January 2007. – 139 p.
25. I. Rokhlin, Dale E.Chimenti, Peter B. Nagy, "Physical Ultrasonic of Composites". Oxford University Press, USA; 1 edition, February 16, 2011. –400p.
26. G. Wrobel, S. Pawlak, "A comparison study of the pulse-echo and through-transmission ultrasonics in glass/epoxy composites". Journal of Achievements in Materials and Manufacturing Engineering, Volume 22, Issue 2, June 2007. – 4 p.

27. Keith Birch, “Estimating Uncertainties in Testing”, An Intermediate Guide to Estimating and Reporting Uncertainty of Measurements in Testing. British Measurement and Testing Association, Addison-Wesley Publishing Company, Inc, London, March 2003. – 44 p.

28. Guidance Document for Estimation of Measurement Uncertainty in Non-Destructive Testing. Accreditation Scheme for Laboratories, Guidance Notes NDT, Singapore, 4 February 2001. – 11 p.

29. Drd. Ing. Diana Mihaela Tesileanu, prof. univ. ing. Lidia Niculita, “The calculating procedure for measurement uncertainty using ultrasound testing”. The Romanian Review Precision Mechanics, Optics & Mechatronics, 2013, No. 44, Bucharest. – 5 p.

30. Diana Mihaela Tesileanu, Lidia Niculita, “Experimental analysis regarding the measurement uncertainty of welded joints with ultrasound testing”. The Romanian Review Precision Mechanics, Optics & Mechatronics, 2013, No. 44, Bucharest. – 9 p.

31. А.И. Походун, “Экспериментальные методы исследований. Погрешности и неопределенности измерений”. Учебное пособие. СПб: СПбГУ ИТМОб 2006 – 112 с.

APPENDIX

Appendix 1. Scientific article of 12th student's conference E2TA on the topic of "Ultrasonic non-destructive evaluation of dissimilar material joints"